WDR82/PNUTS-PP1 prevents transcription-replication conflicts by promoting RNA POLYMERASE II degradation on chromatin

Landsverk, Helga B.; Sandquist, Lise E.; Bay, Lilli T. E.; Steurer, Barbara; Campsteijn, Coen; Landsverk, Ole J. B.; Marteijn, Jurgen A.; Petermann, Eva; Trinkle-Mulcahy, Laura; Syljuasen, Randi G.

DOI:
10.1016/j.celrep.2020.108469

Cell Reports

Article

WDR82/PNUTS-PP1 Prevents Transcription-Replication Conflicts by Promoting RNA Polymerase II Degradation on Chromatin

Graphical Abstract

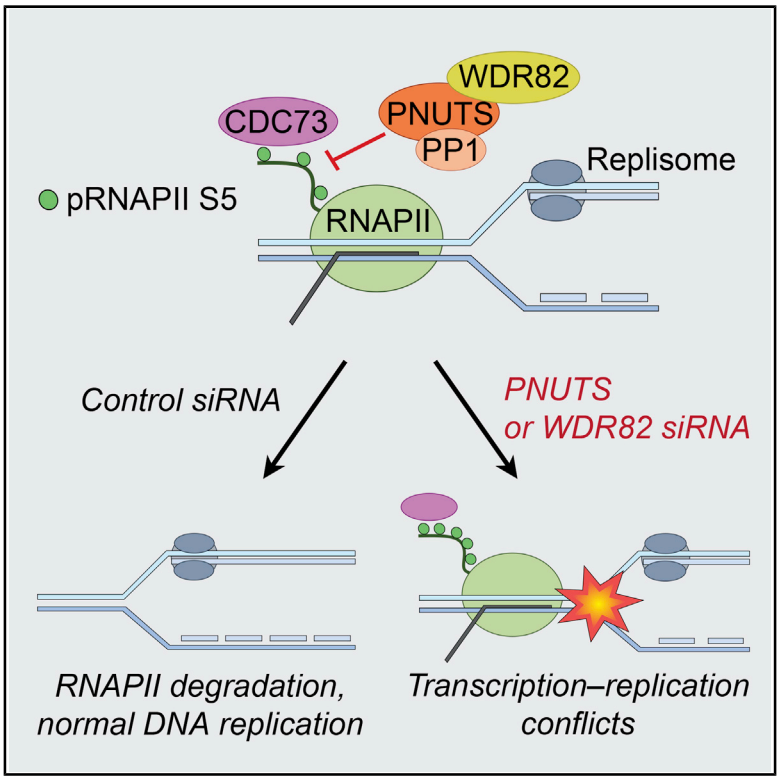

Authors

Helga B. Landsverk, Lise E. Sandquist, Lilli T.E. Bay, ..., Eva Petermann, Laura Trinkle-Mulcahy, Randi G. Syljuåsen

Correspondence

helga.bjarnason.landsverk@rr-research.no (H.B.L.), randi.syljuasen@rr-research.no (R.G.S.)

In Brief

Landsverk et al. show that the RNAPII S5 phosphatase complex WDR82/PNUTS-PP1 suppresses replication stress. WDR82/PNUTS-PP1 promotes degradation of RNAPII on chromatin, thereby reducing the residence time of RNAPII. Their results suggest that proper dephosphorylation of RNAPII is needed to prevent conflicts between transcription and replication.

Highlights

- RNAPII S5 phosphatase PNUTS-PP1 promotes RNAPII turnover on chromatin
- Depletion of PNUTS leads to transcription-replication conflicts
- WDR82 shows similar effects on RNAPII turnover and replication stress as PNUTS
- CDC73 prevents RNAPII degradation and promotes replication stress after PNUTS depletion

Landsverk et al., 2020, Cell Reports *33*, 108469
December 1, 2020
https://doi.org/10.1016/j.celrep.2020.108469

CellPress

Cell Reports

CellPress
OPEN ACCESS

Article

WDR82/PNUTS-PP1 Prevents Transcription-Replication Conflicts by Promoting RNA Polymerase II Degradation on Chromatin

Helga B. Landsverk,[1,7,*] Lise E. Sandquist,[1,7] Lilli T.E. Bay,[1,7] Barbara Steurer,[2] Coen Campsteijn,[5] Ole J.B. Landsverk,[6] Jurgen A. Marteijn,[2] Eva Petermann,[3] Laura Trinkle-Mulcahy,[4] and Randi G. Syljuåsen[1,8,*]

[1]Department of Radiation Biology, Institute for Cancer Research, Norwegian Radium Hospital, Oslo University Hospital, 0379 Oslo, Norway
[2]Department of Molecular Genetics, Oncode Institute, Erasmus MC, University Medical Center Rotterdam, 3015 GE Rotterdam, the Netherlands
[3]Institute of Cancer and Genomic Sciences, College of Medical and Dental Sciences, University of Birmingham, Birmingham B15 2TT, UK
[4]Department of Cellular and Molecular Medicine and Ottawa Institute of Systems Biology, University of Ottawa, Ottawa, ON K1H 8M5, Canada
[5]Department of Molecular Medicine, Institute of Basic Medical Sciences, University of Oslo, 0372 Oslo, Norway
[6]Department of Pathology, Oslo University Hospital, 0372 Oslo, Norway
[7]These authors contributed equally
[8]Lead Contact
*Correspondence: helga.bjarnason.landsverk@rr-research.no (H.B.L.), randi.syljuasen@rr-research.no (R.G.S.)
https://doi.org/10.1016/j.celrep.2020.108469

SUMMARY

Transcription-replication (T-R) conflicts cause replication stress and loss of genome integrity. However, the transcription-related processes that restrain such conflicts are poorly understood. Here, we demonstrate that the RNA polymerase II (RNAPII) C-terminal domain (CTD) phosphatase protein phosphatase 1 (PP1) nuclear targeting subunit (PNUTS)-PP1 inhibits replication stress. Depletion of PNUTS causes lower EdU uptake, S phase accumulation, and slower replication fork rates. In addition, the PNUTS binding partner WDR82 also promotes RNAPII-CTD dephosphorylation and suppresses replication stress. RNAPII has a longer residence time on chromatin after depletion of PNUTS or WDR82. Furthermore, the RNAPII residence time is greatly enhanced by proteasome inhibition in control cells but less so in PNUTS- or WDR82-depleted cells, indicating that PNUTS and WDR82 promote degradation of RNAPII on chromatin. Notably, reduced replication is dependent on transcription and the phospho-CTD binding protein CDC73 after depletion of PNUTS/WDR82. Altogether, our results suggest that RNAPII-CTD dephosphorylation is required for the continuous turnover of RNAPII on chromatin, thereby preventing T-R conflicts.

INTRODUCTION

Faithful DNA replication is essential to maintain genome integrity during cell division. However, problems during DNA replication (i.e., replication stress) can arise from many sources (Gaillard et al., 2015). Replication stress contributes to cancer development (Forment and O'Connor, 2018; Gaillard et al., 2015) and may also be exploited in clinical therapy to selectively kill cancer cells (Forment and O'Connor, 2018; Sørensen and Syljuåsen, 2012). Identification of the molecular mechanisms underlying replication stress is therefore of great significance.

Transcription-replication (T-R) conflicts are a major source of replication stress (Gómez-González and Aguilera, 2019). Sharing the same template, RNA and DNA polymerases may interfere with each other, and such interference (i.e., T-R conflicts) can cause replication stress and genome instability (Gaillard and Aguilera, 2016; Gómez-González and Aguilera, 2019). Interestingly, T-R conflicts are enhanced by oncogenic RAS and CYCLIN E and the breast-cancer-inducing hormone estrogen (Jones et al., 2013; Kotsantis et al., 2016; Stork et al., 2016) and may thus also be involved in cancer development. T-R conflicts can create replication stress by transcription-induced chromatin alterations or topological stress (Gómez-González and Aguilera, 2019). Furthermore, transcription can lead to formation of nucleic acid structures such as R-loops, which can cause both replication stress and genome instability (Hamperl et al., 2017; Lang et al., 2017). R-loops are thus a characteristic of T-R conflicts, and overexpression of RNaseH1, which degrades the RNA strand in RNA-DNA hybrids, can promote replication fork progression in cells with replication stress caused by T-R conflicts (Hodroj et al., 2017; Klusmann et al., 2018; Kotsantis et al., 2016).

RNA polymerase II (RNAPII) pervasively transcribes the genome (Jensen et al., 2013) and has a high potential for creating a physical barrier for DNA replication by itself (Gómez-González and Aguilera, 2019). Indeed, the bacterial replisome pauses upon encountering bacterial RNA polymerase (RNAP) in a head-on conflict (Liu and Alberts, 1995). Furthermore, the

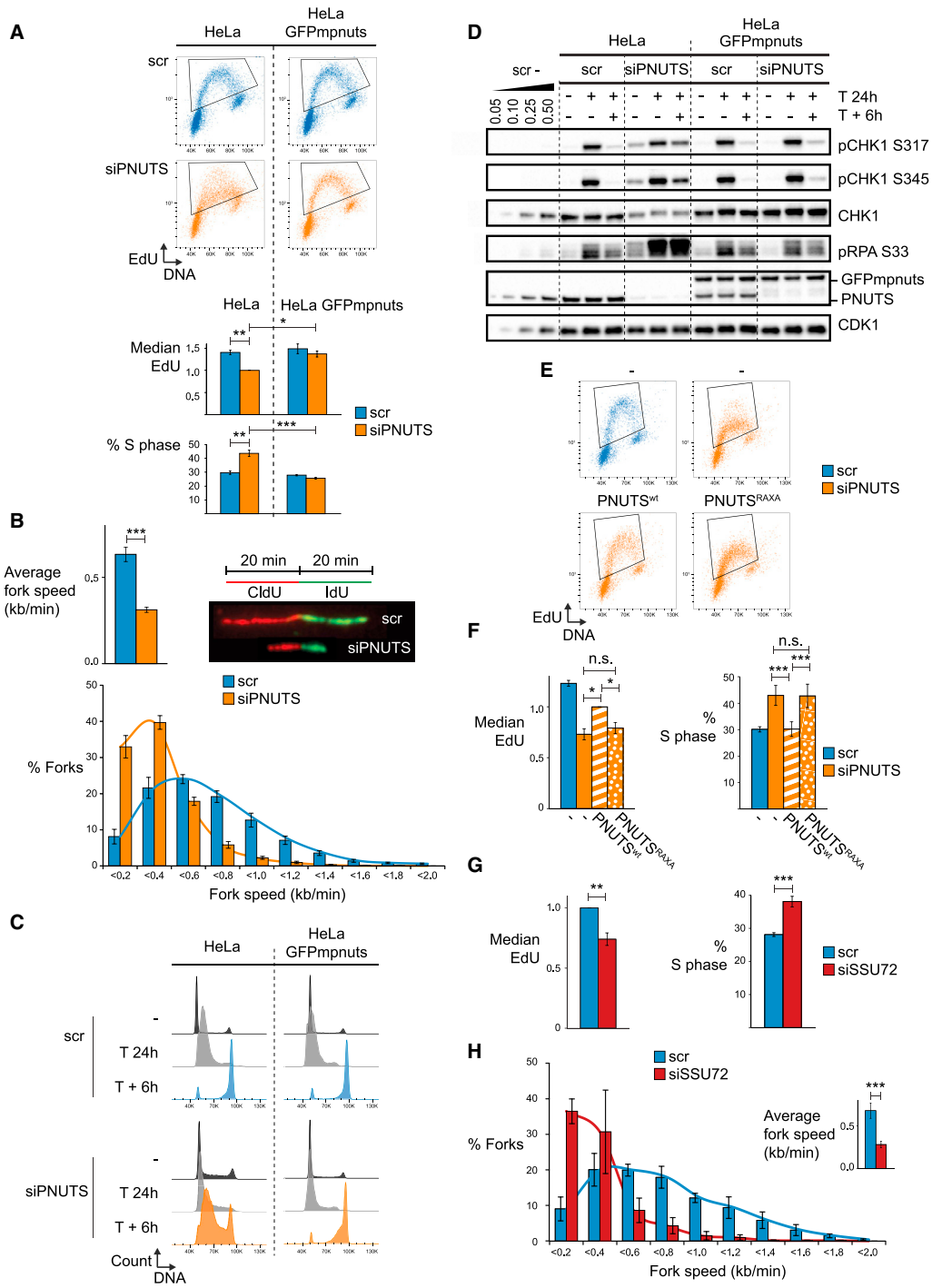

Figure 1. The pRNAPII S5 Phosphatase PNUTS-PP1 Promotes DNA Replication

(A) Flow cytometry analysis of EdU incorporation in HeLa cells or HeLa bacterial artificial chromosome (BAC) clones stably expressing EGFP mouse pnuts (HeLa GFPmpnuts) at 72 h after transfection with siRNA targeting human PNUTS (siPNUTS) or control siRNA (scr). Bottom charts show mean median EdU levels and percentage of cells in S phase (indicated by regions in scatterplots) (n = 3). p value for percentage of cells in S phase was determined by the two-tailed Student's one-sample t test.

(B) DNA fiber analysis of HeLa cells 48 h after transfection with scr or siPNUTS. Representative images of obtained fibers, mean replication fork speed, and distributions of replication fork speed are shown (n = 6). p value was determined by the Wilcoxon signed rank test.

(C) Flow cytometry analysis of HeLa and HeLa GFPmpnuts cells transfected as in (A) and stained with Hoechst 33258. Indicated samples were treated with thymidine (T) for 24 h (T 24 h). In T + 6 h samples, thymidine was removed, and fresh media was added for 6 h.

(legend continued on next page)

transcription-coupled repair factor Mfd and the accessory helicases Rep and UvrD promote replication in bacteria by displacing stalled RNAP (Hawkins et al., 2019; Pomerantz and O'Donnell, 2010). In addition, RNAPII mutants in yeast, which promote the retention of RNAPII on chromatin, display impaired replication fork progression and enhanced genome instability (Felipe-Abrio et al., 2015). These findings imply that a dynamic association of RNAPII with chromatin is required to prevent T-R conflicts. However, at least in human cells, the factors involved remain poorly understood.

During the transcription cycle, RNAPII becomes post-transcriptionally modified in its C-terminal domain (CTD), which is a large unstructured domain consisting of 52 heptapeptide repeats in humans (Harlen and Churchman, 2017). The modifications of the CTD regulate its association with factors involved in initiation, elongation, RNA processing, and termination (Bentley, 2014; Custódio and Carmo-Fonseca, 2016). The most well-known modifications of the CTD are phosphorylation on serine (S)2 (pRNAPII S2) and S5 (pRNAPII S5). Though previously thought to be primarily associated with promoter proximal regions, pRNAPII S5 is also found in gene-internal regions and is particularly enriched on paused RNAPII at splice sites (Nojima et al., 2015). pRNAPII S2 is low at promoter-proximal regions and is associated with elongation and termination (Ahn et al., 2004; Harlen and Churchman, 2017). The CTD also responds to stress such as UV DNA damage, when it becomes extensively hyperphosphorylated (Rockx et al., 2000). Whether the CTD is involved in replication stress is not known. However, several CTD binding proteins are required for resistance to the replication stress inducer doxorubicin (Winsor et al., 2013), indicating such a connection.

Protein phosphatase 1 (PP1) is a major serine threonine phosphatase whose specificity is mediated by regulatory proteins (Boens et al., 2013). PP1 nuclear targeting subunit (PNUTS) is an abundant nuclear PP1 regulatory protein (Kreivi et al., 1997), and its only established substrate is S5 in the CTD of RNAPII (pRNAPII S5) (Ciurciu et al., 2013; Lee et al., 2010). We previously found that PNUTS is involved in the G2 checkpoint and ataxia telangiectasia and Rad3 related (ATR) signaling (Landsverk et al., 2010, 2019). Our results suggested that ATR can be activated via the CTD of RNAPII (Landsverk et al., 2019). Here, we present evidence that PNUTS-PP1-mediated dephosphorylation of RNAPII CTD suppresses T-R conflicts by promoting degradation of RNAPII on chromatin, thus reducing its residence time. Furthermore, we show that WDR82, a major PNUTS interacting partner, shows similar effects. The phenotypes of PNUTS and WDR82 depletion on both replication and the RNAPII residence time on chromatin are dependent on the phospho-CTD binding protein CDC73, a component of the PAF1 transcription elongation complex. Altogether, our results provide insight into how regulation of the transcription machinery contributes to suppression of T-R conflicts in human cells.

RESULTS

PNUTS-PP1 Is Required for DNA Replication under Normal and Stressed Conditions

In our previous work, we observed an increased fraction of cells in S phase and reduced 5-ethynyl-2′-deoxyuridine (EdU) incorporation after small interfering RNA (siRNA)-mediated depletion of PNUTS in HeLa cells, suggesting PNUTS is required for normal DNA replication (Landsverk et al., 2019). These effects were specifically caused by depletion of PNUTS, as they were rescued in cells expressing mouse GFPpnuts (GFPmpnuts) (Figure 1A), which is not affected by human PNUTS siRNA (PNUTS blot in Figure 1D). In addition, PNUTS depletion strongly reduced replication fork rates compared to control siRNA transfected cells (Figure 1B). A higher fraction of S phase cells after depletion of PNUTS was also observed in U2OS cells (Figure S1A). Moreover, PNUTS depletion induced slower recovery from thymidine-induced replication stalling, as more cells transfected with control siRNA had reached the G2/M transition 6 h after release from thymidine than cells transfected with PNUTS siRNA (Figure 1C). The reduced recovery from thymidine-induced replication stalling was also observed in U2OS cells (Figure S1B) and was a specific effect after PNUTS depletion (Figure 1C). Interestingly, a screen searching for factors necessary for recovery from hydroxyurea (HU)-induced replication stalling identified PNUTS among the candidate hits (Sirbu et al., 2013). In line with a role after HU, more PNUTS-depleted cells accumulated in S phase after HU treatment than control siRNA transfected cells (Figure S1C). Consistent with our own previous findings (Landsverk et al., 2019), enhanced ATR signaling was observed after PNUTS siRNA transfection, as measured by increased phosphorylation of CHK1 on S317 and S345 and RPA32 on S33 (Figures 1D and S1D). ATR signaling after depletion of PNUTS was further enhanced by thymidine and was also rescued by GFPmpnuts (Figures 1D and S1D). Moreover, the higher ATR signaling in PNUTS-depleted cells correlated with reduced recovery from replication stalling and a higher percentage of cells with high levels of the DNA damage marker γH2AX at 6 h after release from thymidine block (Figures 1C, 1D, and S1E). To address whether the high ATR activity after depletion of PNUTS was responsible for the effects on replication, we added the ATR inhibitor VE822 (Fokas et al., 2012). Neither EdU uptake nor replication fork rate was reversed by VE822 (Figures S1F and S1G),

(D) Western blot of experiment as in (C).
(E) Flow cytometry analysis as in (A) of HeLa cells 48 h after transfection with scr or siPNUTS. EGFP PNUTS ($PNUTS^{wt}$) or PP1-binding deficient EGFP PNUTS ($PNUTS^{RAXA}$) were transfected at 24 h post-siRNA transfection.
(F) Mean median EdU incorporation or percentage of S phase cells from experiments as in (E) (n = 3).
(G) Mean median EdU incorporation and percentage of cells in S phase from experiments as in (A) of HeLa cells transfected with scr or siRNA targeting SSU72 (siSSU72) (n = 4).
(H) DNA fiber analysis of HeLa cells 48 h after transfection with scr or siSSU72. Average replication fork speed and distributions of replication fork speed are shown. (n = 3). p value was determined by the two-tailed Student's one-sample t test.
Error bars represent SEM. See also Figure S1.

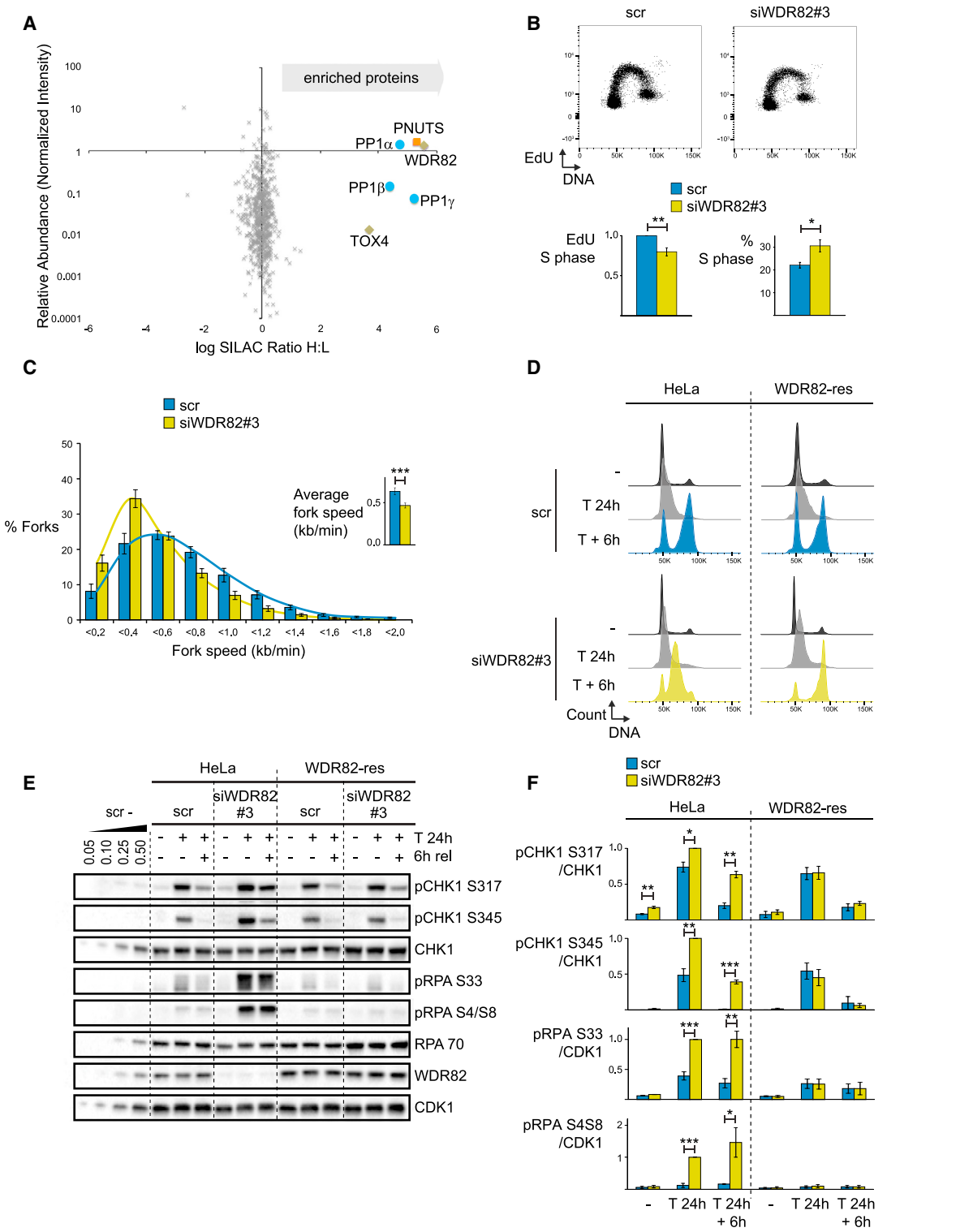

Figure 2. WDR82, a Major PNUTS Interaction Partner, Also Promotes DNA Replication

(A) HeLa cells were isotopically labeled by growth in SILAC media and transiently transfected with PNUTS-EGFP or empty EGFP. After 24 h, lysates were prepared and mixed at a 1:1 ratio. Complexes containing EGFP were isolated, separated by 1D SDS-PAGE, trypsin digested, and analyzed by liquid chromatography-tandem mass spectrometry (LC-MS/MS). Proteins were identified and SILAC ratios and relative abundance quantified using MaxQuant.

(B) Flow cytometry analysis (as in Figure 1A) at 72 h after transfection with scr or siRNA against WDR82 (siWDR82#3) (n = 5).

(legend continued on next page)

suggesting ATR activity is not the main cause of the suppressed replication after depletion of PNUTS. We further addressed whether PP1 was involved by overexpressing a siRNA-resistant PP1 binding deficient mutant (EGFP PNUTS^{RAXA}). While wild-type PNUTS (EGFP PNUTS^{wt}) partially rescued the lower EdU uptake and completely rescued the enhanced S phase fraction after depletion of endogenous PNUTS, EGFP PNUTS^{RAXA} did not (Figures 1E and 1F). The dependency on PP1 suggested that reduced pRNAPII S5 dephosphorylation might be causing the effects of PNUTS depletion on replication. Supporting this, depletion of another pRNAPII S5 phosphatase, SSU72 (Krishnamurthy et al., 2004), also reduced EdU incorporation and replication fork speed and enhanced the S phase fraction (Figures 1G, 1H, and S3B). Together, these findings show that PNUTS-PP1 is required for normal replication fork progression and suggest it does so by dephosphorylating pRNAPII S5.

WDR82, a PNUTS Interaction Partner, Is Also Required for DNA Replication under Normal and Stressed Conditions

To search for additional PNUTS binding partners that might contribute to the role of PNUTS-PP1 in DNA replication, we performed stable isotope labeling of amino acids in cell culture (SILAC) immunoprecipitation (IP) of PNUTS EGFP followed by mass spectrometry (Figure 2A). This method allows the identification of high confidence protein interactions, as it enables subtraction of background and bait interactions (Trinkle-Mulcahy, 2012). The major PNUTS interaction partners identified were WDR82, TOX4 and the PP1 isoforms; PP1α, PP1β, and PP1γ (Figure 2A; Table S1). The PNUTS/TOX4/WDR82 (PTW)-PP1 complex has also been reported by others (Lee et al., 2010). We verified the interactions by coIP using EGFP-tagged PNUTS, mpnuts, TOX4, WDR82, PP1α, PP1β, and PP1γ (Figures S2A–S2E; data not shown). Consistent with PNUTS acting as a scaffolding protein in the PTW-PP1 complex (Lee et al., 2010), depletion of WDR82 did not reduce association of EGFP mpnuts with PP1γ or TOX4 (Figure S2D), and PP1 binding was not required for the association between PNUTS and WDR82 or TOX4 (Figures S2A and S2C). As WDR82 binds directly to pRNAPII S5 (Lee and Skalnik, 2008), we addressed whether WDR82 might also play a role in DNA replication. Indeed, siRNA-mediated depletion of WDR82 reduced EdU incorporation and increased the fraction of cells in S phase compared to control siRNA transfected cells (Figure 2B). Supporting that PNUTS and WDR82 are acting in the same pathway, co-depletion of WDR82 with PNUTS did not show additive effects on EdU uptake or the S phase fraction (Figures S3A and S3B). Depletion of WDR82 also reduced replication fork speed, reduced recovery from replication stalling, and enhanced ATR signaling with and without thymidine (Figures 2C–2F, S2F, and S2G). The effects on recovery from replication stalling and ATR signaling were specific for WDR82, as they were rescued by siRNA-resistant WDR82 (Figures 2D–2F, S2F, and S2G). Enhanced ATR signaling was also observed with two additional siRNA oligonucleotides (Figures S2H and S2I). Furthermore, WDR82 depletion caused higher accumulation in S phase after HU and more RPA loading and higher levels of γH2AX and pRPA S4S8 24 h after thymidine (Figures 2E, 2F , and S3C–S3E), suggesting WDR82 is required to prevent DNA damage and promotes cell survival during replication stress. Supporting this, WDR82 depletion reduced cell survival after hydroxyurea treatment (Figure S3F).

WDR82 Facilitates pRNAPII S5 Dephosphorylation by PNUTS-PP1 in Live Cells

We further addressed whether WDR82 plays a role in dephosphorylation of pRNAPII S5. Indeed, WDR82 depletion specifically enhanced levels of pRNAPII S5 (Figures 3A, 3B, and S2I). Previously, we used the CDK7 inhibitor THZ1 to show that PNUTS-PP1 plays a major role in pRNAPII S5 dephosphorylation during replication stress (Landsverk et al., 2019). Remarkably, we obtained similar results with WDR82. While pRNAPII S5 was reduced after THZ1 treatment in control siRNA transfected cells, it was not reduced in cells transfected with WDR82 siRNA (Figures 3C and 3D), supporting a role for WDR82 in pRNAPII S5 dephosphorylation. To further explore this, we performed an *in vitro* dephosphorylation assay. Using RNAPII bound to GFPmpnuts as a substrate, we confirmed that pRNAPII S5 is a direct substrate for PNUTS-PP1 (Figures 3E and 3F; Ciurciu et al., 2013; Lee et al., 2010). pRNAPII S5 was selectively dephosphorylated compared to pRNAPII S2 (Figures 3E and 3F), showing that PNUTS-PP1 displays specificity for pRNAPII S5 versus pRNAPII S2 *in vitro*. Furthermore, PP1 was the phosphatase involved, as calyculin A, a PP1 inhibitor (Swingle et al., 2007), inhibited pRNAPII S5 dephosphorylation (Figure 3E). Though depletion of WDR82 reduced the amount of WDR82 in the GFPmpnuts pull-downs, the rate of pRNAPII S5 dephosphorylation was unaltered compared to controls (Figures 3E and 3G). Thus, though WDR82 is required for pRNAPII S5 dephosphorylation in live cells, it may not be required for its dephosphorylation *in vitro*. Alternatively, the small remaining amount of WDR82 (Figure 3E) may be sufficient for *in vitro* dephosphorylation of pRNAPII S5. Supporting a requirement for WDR82 in mediating RNAPII dephosphorylation in live cells, a higher amount of RNAPII relative to GFPmpnuts was pulled down from WDR82-depleted versus control siRNA transfected cells (Figure 3E, time 0 min, and Figure 3H). Moreover, the amount of RNAPII relative to PP1γ was also higher (Figure 3E, time 0 min, and Figure 3I). This is reminiscent of the increased interaction between pRNAPII S5 with a hypoactive PNUTS-PP1 fusion mutant observed in pull-downs from HEK293T cells (Wu et al., 2018) and is thus highly consistent with a dephosphorylation defect.

(C) DNA fiber analysis of HeLa cells 48 h after transfection with scr or siWDR82#3 as in Figure 1B. p value was determined by the Wilcoxon signed rank test (n = 6).
(D) Flow cytometry analysis (as in Figure 1C) of HeLa or HeLa cells stably expressing siRNA-resistant WDR82 (WDR82-res) 72 h after transfection with scr or siWDR82#3.
(E) Western blot of experiment as in (D).
(F) Mean results from experiments as in (E) (n = 3).
Error bars represent SEM. See also Figures S2 and S3 and Table S1.

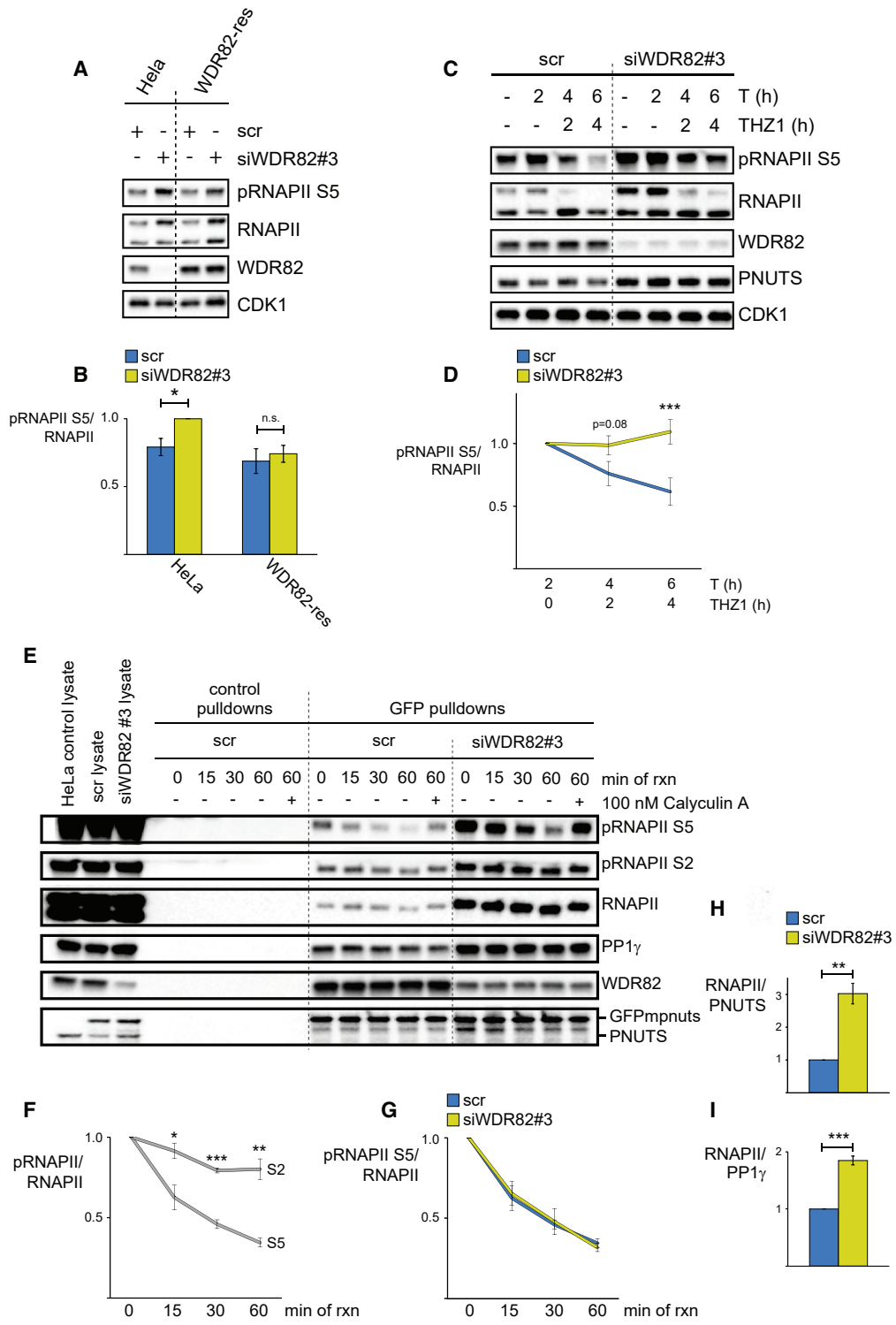

Figure 3. WDR82 Facilitates pRNAPII S5 Dephosphorylation by PNUTS-PP1 in Live Cells

(A) Western blot of HeLa or WDR82-res cells 72 h after siRNA transfection with scr or siWDR82#3.

(B) Mean pRNAPII S5 versus RNAPII from experiments as in (A). p values were determined by the two-tailed Student's one-sample t test (n = 7).

(C) Western blot analysis of scr or siWDR82#3 transfected HeLa cells treated with thymidine (T) for 2, 4, and 6 h. THZ1 was added 2 h after thymidine treatment.

(D) Mean fold changes of pRNAPII S5 relative to RNAPII for THZ1 and thymidine samples relative to the T 2 h sample from experiments as in (C) (n = 8). Statistical significance was determined from fold changes in scr versus siWDR82#3 samples at indicated time points.

(legend continued on next page)

Depletion of PNUTS or WDR82 Enhances the Residence Time of Phosphorylated RNAPII on Chromatin

T-R conflicts can occur due to enhanced retention of RNAPII on chromatin (Chakraborty et al., 2018; Felipe-Abrio et al., 2015; Poli et al., 2016). Thus, one hypothesis might be that defective p-RNAPII S5 dephosphorylation could lead to alterations in the dynamics of RNAPII, causing T-R conflicts. We addressed this by fluorescence recovery after photobleaching (FRAP) analysis of GFP RNAPII in MRC5 cells (Steurer et al., 2018). PNUTS depletion caused a larger immobile fraction of GFP RNAPII (Figure 4A), indicating a larger fraction of RNAPII complexes were stably chromatin bound. Of note, the levels of GFP RNAPII were lower after PNUTS depletion compared to control siRNA transfected cells (Figure S4A). We further explored this by assessing the chromatin residence time of transcriptionally engaged RNAPII. To do so, we measured the decrease in RNAPII chromatin binding after THZ1 treatment, which prevents *de novo* transcription initiation (Steurer et al., 2018) and pRNAPII S5 phosphorylation (Kwiatkowski et al., 2014). Supporting inhibition of *de novo* transcription initiation by THZ1, a reduction of chromatin-bound RNAPII was observed both in PNUTS-depleted and in control siRNA transfected cells after THZ1 treatment during thymidine-induced replication stress (Figures 4B and 4C). However, RNAPII on chromatin was less reduced in cells depleted of PNUTS (reduced by 42%) compared to control siRNA transfected cells (reduced by 72%) (Figures 4B and 4C), consistent with higher residence time of chromatin-bound RNAPII. Furthermore, pRNAPII S5 was also less reduced in PNUTS-depleted cells after THZ1 treatment (Figure 4B and 4D). These results were further extended by high-precision flow cytometry analysis of detergent-extracted cells, which confirmed the higher residence time of pRNAPII S5 on chromatin with THZ1 after PNUTS depletion, both in the presence and absence of thymidine (Figures 4E, 4G, 4H, S4B, S4D, and S4F). Furthermore, similar results for pRNAPII S5 were found in WDR82-depleted cells (Figures 4E, 4G, 4H, S4B, and S4D). Notably, flow cytometry also allowed the distinction between G1 and S phases of the cell cycle based on DNA content, and for pRNAPII S5, similar effects were observed in both phases (Figures 4H and S4D). Using an antibody that recognizes the N terminus of RNAPII, we confirmed that levels of total RNAPII were reduced by THZ1 on chromatin in PNUTS and WDR82 depleted and in control siRNA transfected cells (Figures 4F, 4I, S4C, and S4E). Moreover, though the differences were smaller than with pRNAPII S5, total RNAPII chromatin loading was significantly less reduced by THZ1 after depletion of PNUTS or WDR82, at least in G1 phase (Figure 4I). These results show that RNAPII has a higher residence time on chromatin after depletion of PNUTS or WDR82. We reasoned that this was likely caused by defective dephosphorylation of pRNAPII S5. Supporting this, while EGFP PNUTS^{wt} partially rescued the lower reduction in chromatin binding of pRNAPII S5 and RNAPII after THZ1 in PNUTS siRNA transfected cells, EGFP PNUTS^{RAXA} rescued less (Figures 4J, 4K, S4G, and S4H). Furthermore, depletion of SSU72 also suppressed the reduction in pRNAPII S5 and RNAPII on chromatin after THZ1 (Figure 4L). As depletion of two different pRNAPII S5 phosphatases show similar effects, these results suggest that defective dephosphorylation of pRNAPII S5 underlies the enhanced residence time of RNAPII on chromatin.

CDC73 Is Required to Enhance the Residence Time of Phosphorylated RNAPII on Chromatin and for Suppression of Replication after Depletion of PNUTS or WDR82

We previously found that CDC73, a component of the PAF1 transcription elongation complex which binds the phospho-CTD (Qiu et al., 2012), was required for high ATR activity after depletion of PNUTS (Landsverk et al., 2019). To address whether it also plays a role in the replication phenotypes and the enhanced RNAPII-residence time on chromatin, we co-depleted CDC73 with PNUTS. Co-depletion of CDC73 partially reversed the enhanced residence time of RNAPII on chromatin, as RNAPII and pRNAPII S5 were more reduced after THZ1 in cells co-depleted of CDC73 and PNUTS compared to cells transfected with PNUTS siRNA alone (Figures 5A–5F and S5A–S5C). Co-depletion of CDC73 with PNUTS also partially reversed the slower replication fork rate and EdU uptake in PNUTS depleted cells, while depletion of CDC73 alone did not alter the replication fork rate compared to control siRNA transfected cells (Figures 5G, 5H, S5D, and S5E). Moreover, the enhanced EdU uptake upon co-depletion of CDC73 with PNUTS was a specific effect of the CDC73 siRNA, as it was rescued in cells expressing siRNA-resistant CDC73 (Figures 5H, S5D, and S5E). Co-depletion of CDC73 also reversed the effects on replication after depletion of WDR82, as it suppressed the enhanced accumulation of cells in S phase after a low dose of hydroxyurea observed in cells depleted of WDR82 alone (Figure S5F). Together, these results show CDC73 is required for the prolonged residence time of phosphorylated RNAPII on chromatin and for suppression of replication after depletion of PNUTS and WDR82.

Enhanced Chromatin Retention of RNAPII Is Due to Reduced Degradation on Chromatin after Depletion of PNUTS or WDR82

During the chromatin extractions, we noticed that though the levels of RNAPII decreased on chromatin with THZ1, they did not increase in the corresponding soluble fractions (Figures 6A and 6B). This indicated that RNAPII was being degraded at or

(E) Western blot of a phosphatase assay using RNAPII pulled down with GFPmpnuts as substrate. HeLa GFPmpnuts or HeLa cells (used for control pull-downs) were harvested 72 h after transfection with scr or siWDR82#3. Isolated GFP complexes were incubated at 30°C for the indicated times in the presence or absence of 100 nM calyculin A.

(F) Mean fold changes of pRNAPII/RNAPII for S2 and S5 relative to the t = 0 min sample from (E) in complexes from cells transfected with scr. Statistical significance was determined from fold changes of pRNAPII S2/RNAPII versus pRNAPII S5/RNAPII at indicated time points (n = 3).

(G) As in (F) except showing fold changes of pRNAPII S5/RNAPII in complexes from cells transfected with scr and siWDR82#3.

(H) Mean RNAPII relative to GFPmpnuts in complexes from cells transfected with scr or siWDR82#3 as in (E) at t = 0 min. (n = 3).

(I) As in (H) except showing RNAPII relative to PP1γ.

p values in (H) and (I) were determined by the two-tailed Student's one-sample t test. Error bars represent SEM.

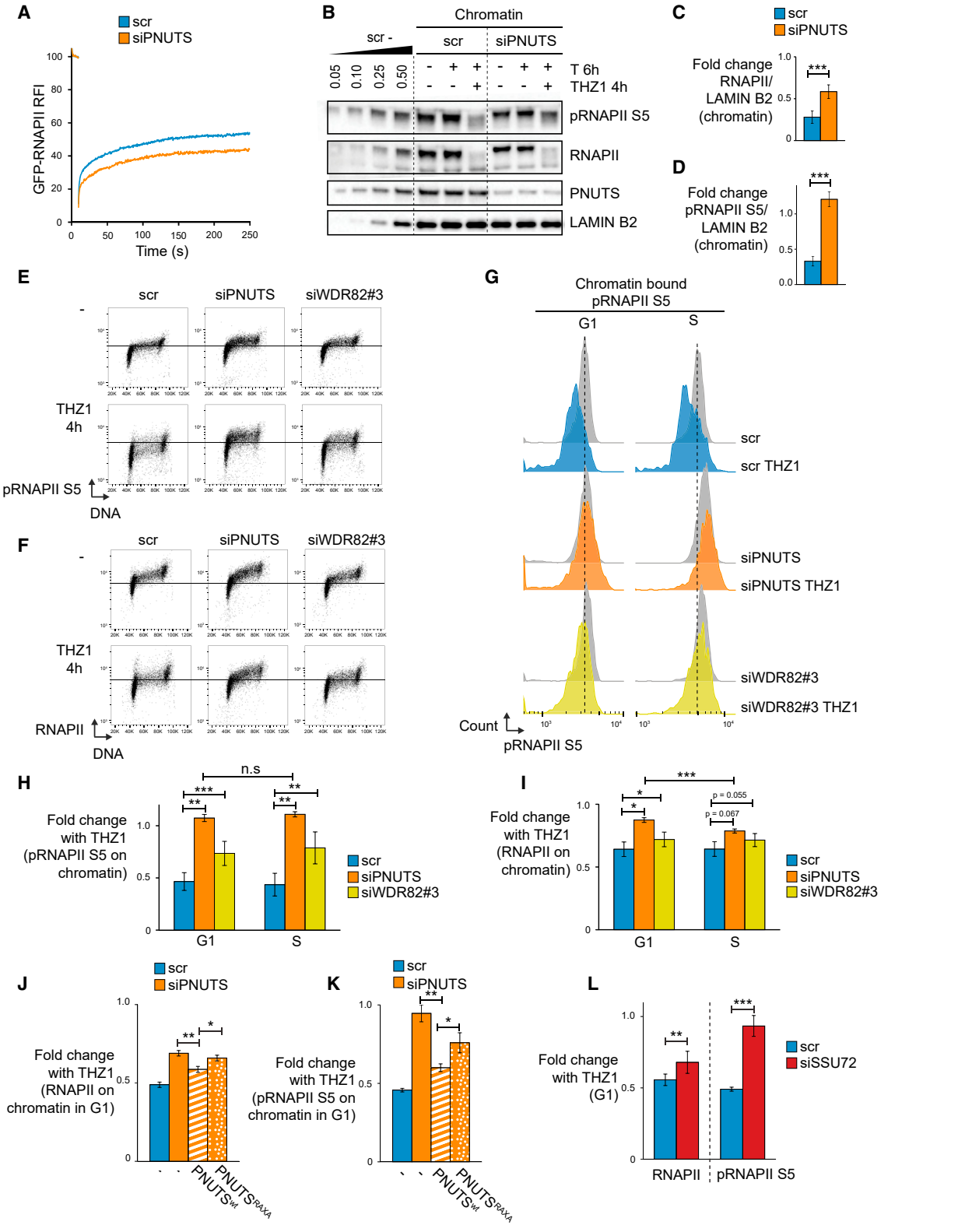

(legend on next page)

in the close vicinity of chromatin during THZ1 treatment. To further address this, we measured the chromatin residence time of RNAPII and pRNAPII S5 after THZ1 treatment with the proteasome inhibitor MG132. Remarkably, in the presence of MG132, the levels of pRNAPII S5 and RNAPII were substantially less reduced by THZ1 in control siRNA transfected cells in both G1 and S phase (Figures 6C–6E). This is consistent with extensive proteasome-mediated degradation of chromatin-bound RNAPII during THZ1 treatment. In contrast, MG132 had a much smaller effect on the levels of RNAPII and pRNAPII S5 in PNUTS-depleted cells (Figures 6C–6G), indicating less proteasome-mediated degradation of chromatin-bound RNAPII. Similar effects were observed after depletion of WDR82 and SSU72 (Figures 6C–6G). Moreover, co-depletion of CDC73 with PNUTS partially reversed the reduced effects of MG132 on RNAPII and pRNAPII S5 levels in cells depleted of PNUTS alone (Figure S5G). Altogether, these results strongly suggest pRNAPII S5 dephosphorylation by WDR82/PNUTS-PP1 is promoting degradation of RNAPII on chromatin, thereby reducing RNAPII residence time.

Phosphorylated RNAPII Promotes T-R Conflicts after Depletion of PNUTS or WDR82

So far, our results were consistent with defective pRNAPII S5 dephosphorylation stabilizing RNAPII by suppressing its degradation on chromatin, and thus enhancing T-R conflicts after depletion of PNUTS or WDR82. To further test this hypothesis, we performed a proximity ligation assay (PLA) with RNAPII and the replication factor proliferating cell nuclear antigen (PCNA) by high-precision flow cytometry (Figures 7A, S6A, and S6B). Supporting more T-R conflicts after depletion of PNUTS, a higher RNAPII-PCNA PLA signal in S phase was observed in PNUTS-depleted cells compared to control cells (Figure 7A). A higher PLA signal could also be observed by fluorescence microscopy (Figure S6C). As we had previously observed increased amounts of R-loops after depletion of PNUTS (Landsverk et al., 2019), we addressed whether R-loops might be involved in the effects on replication. Consistent with T-R conflicts, overexpression of RNaseH1 partially rescued the reduced EdU incorporation and fork rate after depletion of PNUTS (Figures 7B and 7C). In contrast, overexpression of RNaseH1 reduced EdU incorporation and fork rate in control siRNA transfected cells (Figures 7B and 7C). R-loops are thus likely contributing to the reduced replication after depletion of PNUTS. On the other hand, overexpression of RNaseH1 did not rescue the reduced fork rate in cells depleted of WDR82 (Figure 7C). To address whether the higher stability of RNAPII on chromatin might contribute to suppression of replication, we performed the fiber assay after inhibition of *de novo* transcription initiation by THZ1. Remarkably, THZ1 enhanced replication fork rates after depletion of PNUTS and WDR82 (Figure 7D), strongly supporting an involvement of T-R conflicts via the longer residence time of RNAPII on chromatin. In contrast, in control siRNA transfected cells, THZ1 slightly reduced fork rates (Figure 7D). Note that THZ1 treatment had a greater effect on rescuing the reduced fork rates after depletion of WDR82 than PNUTS (Figure 7D). Indeed, this may reflect the difference in severity of the effects after depletion PNUTS versus WDR82 on replication and RNAPII residence time. Altogether, our results strongly support the hypothesis that dephosphorylation of pRNAPII S5 by WDR82/PNUTS-PP1 suppresses the residence of time RNAPII on chromatin by promoting its degradation, thus preventing T-R conflicts and counteracting replication stress (Figure 7E).

DISCUSSION

Replication stress is common in cancer cells and can be caused by T-R conflicts (Gaillard and Aguilera, 2016; Gaillard et al., 2015). The mechanisms that regulate transcription to prevent T-R conflicts have until now remained obscure. In this work, we describe a pathway involving a main signaling platform of transcription, namely the CTD, that promotes degradation of RNAPII on chromatin and counteracts replication stress. Our work identifies an important role for RNAPII-CTD dephosphorylation in suppressing replication stress during normal transcription. As reduced dephosphorylation of the CTD prevented proteasome-mediated degradation of RNAPII and caused

Figure 4. Depletion of PNUTS or WDR82 Enhances the Residence Time of Phosphorylated RNAPII on Chromatin

(A) FRAP analysis of GFP-RNAPII knockin MRC5 cells transfected with siPNUTS or scr. GFP-RNAPII was bleached in a narrow strip spanning the nucleus. Fluorescence recovery was measured every 0.4 s for 4 min, background corrected, and normalized to prebleach fluorescence intensity. Mean values of n = 32 cells from three independent experiments are shown.

(B) Western blot analysis of chromatin fractions from cells at 48 h after transfection with scr or siPNUTS. Thymidine was added at 6 h and THZ1 at 4 h prior to harvest. LAMIN B2 was used as loading control for chromatin fractions.

(C) Mean fold changes of RNAPII/LAMIN B2 with THZ1 and thymidine relative to thymidine alone in (B) (n = 6).

(D) As in (C) except showing pRNAPII S5/LAMIN B2.

(E) Flow cytometry analysis showing levels of pRNAPII S5 on chromatin versus DNA content 48 h after transfection with scr, siPNUTS, or siWDR82#3 with and without THZ1 (THZ1 4 h). The black line is to ease visual interpretation.

(F) As in (E) except showing levels of RNAPII on chromatin relative to DNA content.

(G) Histograms showing distribution of pRNAPII S5 levels on chromatin in G1 and S phase in individual cells from same experiment as in (E). The dotted line is provided to ease visual interpretation.

(H) Mean fold changes of pRNAPII S5 on chromatin in THZ1-treated relative to nontreated cells in G1 and S phases from experiments as in (E) (n = 3).

(I) As in (H) except showing fold changes in total RNAPII levels.

(J) Mean fold changes of RNAPII on chromatin in THZ1-treated relative to nontreated cells in G1, 48 h after transfection with scr and siPNUTS, and 42 h after transfection with $PNUTS^{wt}$ or $PNUTS^{RAXA}$ (n = 3).

(K) As in (J) except showing pRNAPII S5.

(L) As in (H) and (I), 42 h after transfection with scr and siSSU72 (n = 4).

In this figure, all p values were determined by the two-tailed Student's one-sample t test. Error bars represent SEM. See also Figure S4.

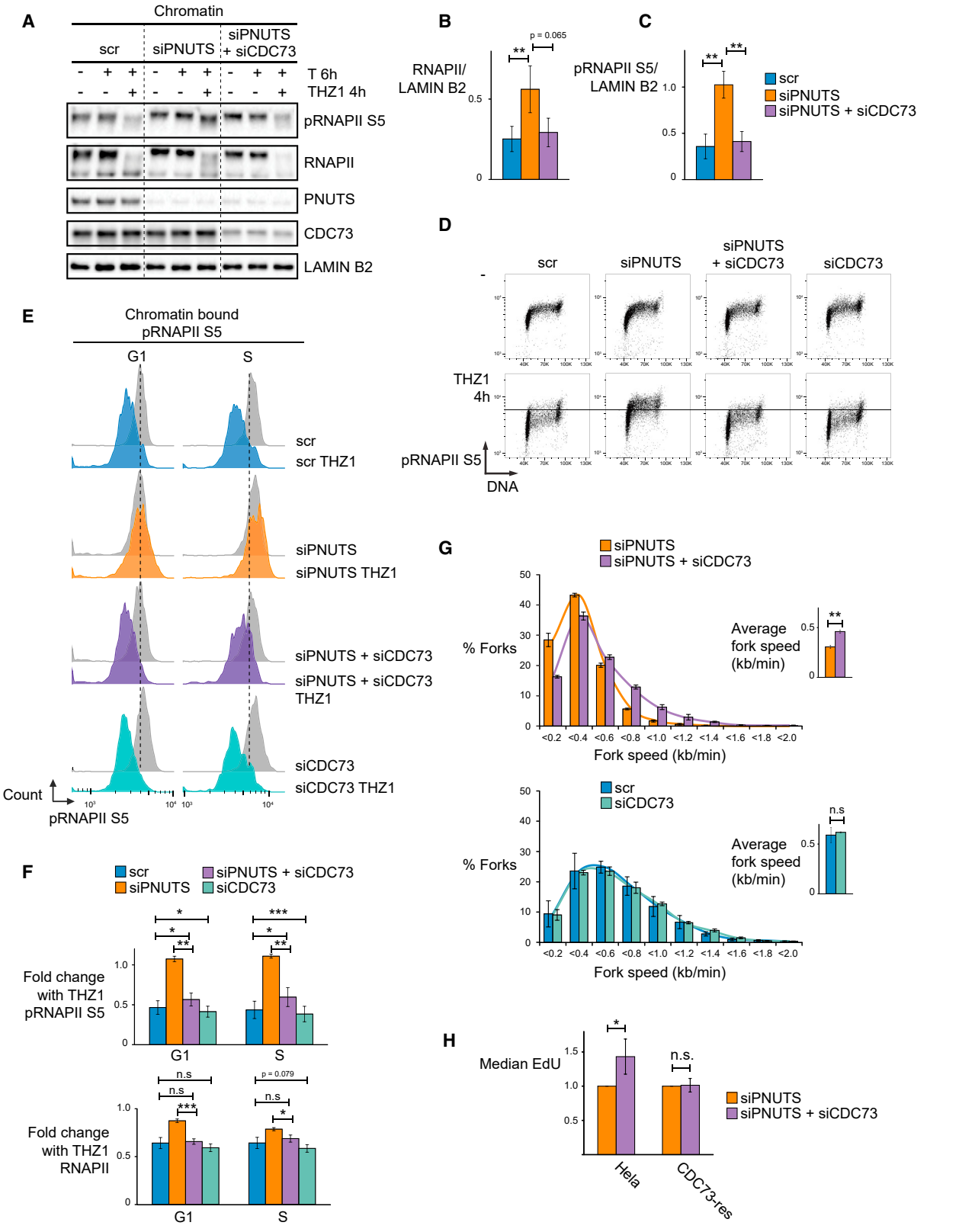

(legend on next page)

replication stress, our results suggest that continuous turnover of RNAPII on chromatin is required to prevent T-R conflicts.

Our results support previous studies suggesting that increased retention of RNAPII on chromatin can cause replication stress and that RNAPII can be removed by degradation during T-R conflicts (Felipe-Abrio et al., 2015; Poli et al., 2016). Our results show that this applies also in human cells and identify several factors involved in regulation of RNAPII turnover to prevent T-R conflicts, namely WDR82/PNUTS-PP1 and pRNAPII S5. A previous study in yeast showed pRNAPII S5 prevented ubiquitinylation and degradation of RNAPII (Somesh et al., 2005), suggesting that the inhibitory role of pRNAPII S5 in RNAPII degradation may be conserved. On the other hand, previous studies in human cells showed that the phosphorylated CTD was associated with increased RNAPII degradation (McKay et al., 2001) and pRNAPII S5 was specifically bound to E3 ubiquitin ligase after DNA damage (Yasukawa et al., 2008). Thus, in human cells, there are likely multiple pathways for RNAPII degradation. In line with this, the stability of RNAPII on chromatin was reduced in S phase compared to G1 phase and pRNAPII S5 was reduced in S phase by addition of thymidine after depletion of PNUTS, but not in control siRNA transfected cells (Figures 4I and S4F). High pressure to remove RNAPII during T-R collisions in PNUTS-depleted cells in S phase may thus promote alternative pathways for RNAPII removal from chromatin.

Though more work is required to understand the conditions under which WDR82/PNUTS-PP1-dependent RNAPII degradation occurs, the following points of evidence suggest it involves elongating RNAPII. First, RNAPII bound to PNUTS was phosphorylated on S2 (Figure 3E), which is associated with elongation. Supporting this, PNUTS colocalizes with pRNAPII S2 in flies and human cells (Ciurciu et al., 2013; Verheyen et al., 2015) and was found throughout the gene body by chromatin IP (ChIP) analysis in human cells (Cortazar et al., 2019). Furthermore, after THZ1 treatment of PNUTS-depleted human cells, phosphorylation of both RNAPII S5 and S2 was prolonged (Landsverk et al., 2019), suggesting that the lack of pRNAPII S5 dephosphorylation might also inhibit dephosphorylation of pRNAPII S2 or, more likely, degradation of S2-phosphorylated elongating RNAPII. Moreover, PNUTS was recently found to be a global decelerator of RNAPII elongation that promotes termination (Austenaa et al., 2015; Cortazar et al., 2019) and WDR82 also has a similar role in termination (Austenaa et al., 2015). Interestingly, termination factors have previously been found to play a role in counteracting replication stress and genome instability, leading to the hypothesis that transcription termination counteracts T-R conflicts (Gómez-González and Aguilera, 2019). Therefore, the more stable, chromatin-bound, phosphorylated RNAPII fraction after depletion of PNUTS or WDR82 may in part represent elongating RNAPII that has failed to terminate and is unable to be removed by degradation.

Notably, transcription termination factors are also connected to R-loop metabolism (Santos-Pereira and Aguilera, 2015). One way termination factors may prevent replication stress could therefore be to remove hazardous R-loops (Santos-Pereira and Aguilera, 2015). As depletion of PNUTS causes R-loops (Landsverk et al., 2019), the enhanced replication stress may therefore be related to R-loops. Supporting this, we found that overexpression of RNaseH1 partially rescued the reduced EdU uptake and fork rate after depletion of PNUTS. On the other hand, while THZ1 completely rescued the fork rate in cells depleted of WDR82, overexpression of RNaseH1 did not. Thus, R-loops may contribute to the reduced replication when pRNAPII S5 dephosphorylation is suppressed by depletion of PNUTS but is unlikely to be the main underlying cause.

CDC73, a tumor suppressor, is a component of the PAF1 transcription elongation complex, which includes WDR61, CDC73, PAF1, LEO1, and CTR9 in humans. Interactions between CDC73, WDR61, and CTR9 with PNUTS have previously been identified (Hein et al., 2015; Landsverk et al., 2019), and CDC73 and WDR61 were putative hits in our SILAC IP (Table S1), suggesting the whole or parts of the PAF complex may functionally interact with WDR82/PNUTS-PP1. Here, we show that CDC73 is required for suppression of replication following depletion of PNUTS or WDR82. CDC73 binding to the phospho-CTD is stimulated by diphosphorylation on S5/S2 or S5/S7 (Qiu et al., 2012). Moreover, CDC73 binds more to RNAPII after depletion of PNUTS (Landsverk et al., 2019). CDC73 may thus partially shield RNAPII from other pRNAPII S5 phosphatases and/or from the proteasome machinery itself. Interestingly, in yeast, CDC73 and the PAF1 complex were required for Mec1 dependent removal of RNAPII during replication stress (Poli et al., 2016), suggesting interspecies differences or multiple pathways for RNAPII degradation.

Here we show that WDR82 and PNUTS counteract replication stress and find several lines of evidence connecting this to their

Figure 5. Co-depletion of CDC73 Reverses Enhanced Residence Time of RNAPII on Chromatin and Replication Effects after Depletion of PNUTS or WDR82

(A) Western blot analysis of chromatin fractions from cells transfected with scr, siPNUTS, or siPNUTS and siRNA against CDC73 (siCDC73) at 48 h after siRNA transfection. Thymidine was added at 6 h and THZ1 at 4 h prior to harvest.

(B and C) Mean fold changes of RNAPII/LAMIN B2 (B) or pRNAPII S5/LAMIN B2 (C) with THZ1 and thymidine relative to thymidine alone from experiments as in (A) (n = 3). p values were determined by the two-tailed Student's one-sample t test.

(D) Flow cytometry analysis of pRNAPII S5 on chromatin in extracted cells 48 h after transfection with scr, siPNUTS, siCDC73, and siPNUTS and siCDC73 with or without THZ1 for 4 h (THZ1 4 h). The black line is shown to ease visual interpretation.

(E) Distribution of pRNAPII S5 levels on chromatin in G1 and S phase in cells from same experiment as in (D).

(F) Mean fold changes of pRNAPII S5 and RNAPII on chromatin in THZ1-treated versus nontreated cells in G1 and S phases. (n = 3). p values were determined by the two-tailed Student's one-sample t test.

(G) DNA fiber analysis performed in HeLa cells 48 h after transfection with scr, siPNUTS, siCDC73, and siPNUTS and siCDC73. Mean distributions of replication fork speed, as well as replication fork speed, are shown (n = 3). p values were determined by the Wilcoxon signed rank test.

(H) Mean median EdU incorporation in HeLa or HeLa cells stably expressing siRNA-resistant CDC73 (CDC73-res) 72 h after siRNA transfection with siPNUTS or siPNUTS and siCDC73 from experiments as shown in Figure S5D. p values were determined by the two-tailed Student's one-sample t test (n = 4).

Error bars represent SEM. See also Figure S5.

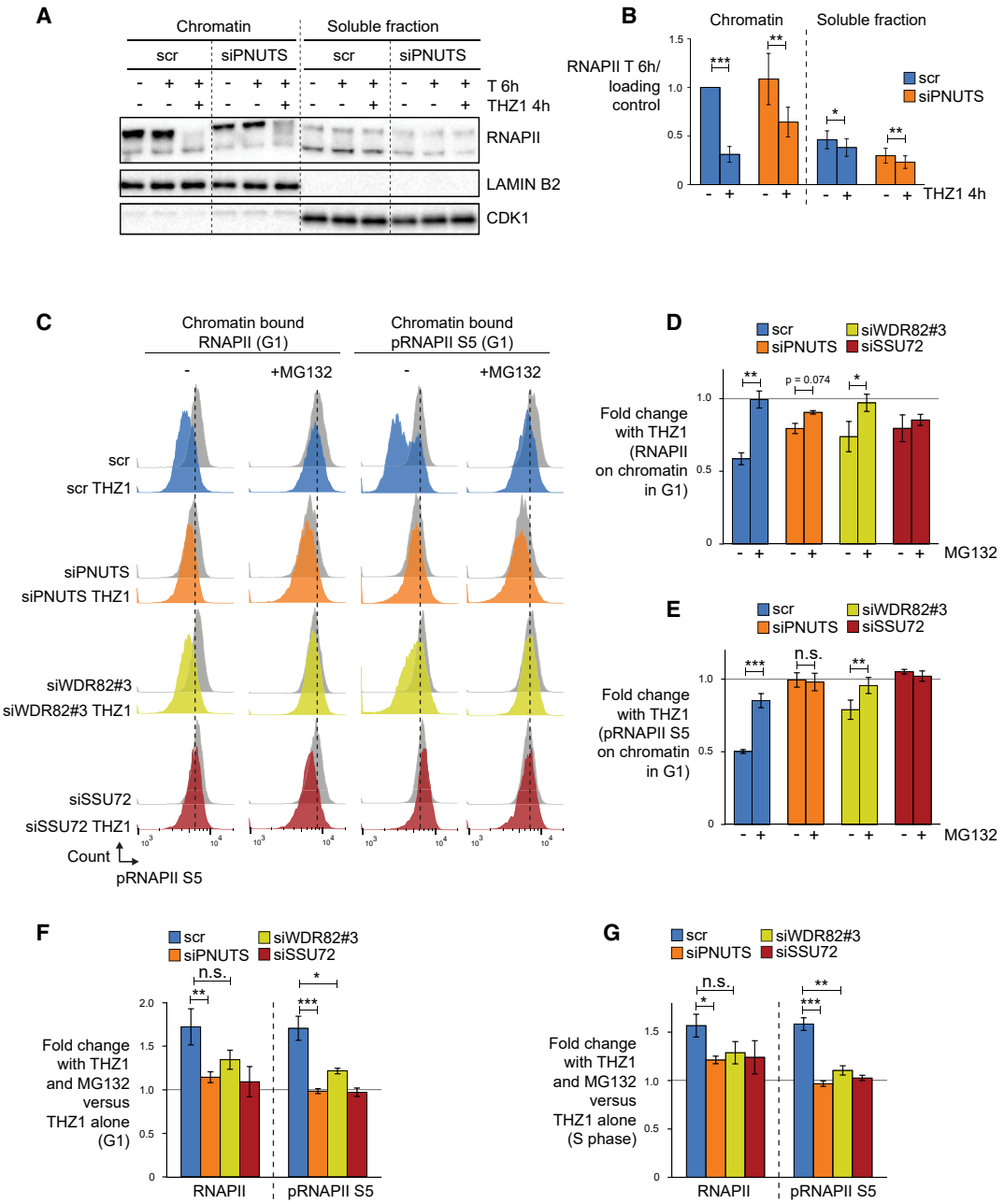

Figure 6. Enhanced RNAPII Chromatin Residence Time Is Caused by Less Proteasome-Mediated Degradation on Chromatin after Depletion of PNUTS or WDR82

(A) Western blot analysis of chromatin and soluble fractions 48 h after transfection with scr or siPNUTS. Thymidine was added at 6 h and THZ1 at 4 h prior to harvest. LAMIN B2 and CDK1 were used as loading controls for chromatin and soluble fractions, respectively.

(B) Mean levels of RNAPII/LAMIN B2 and RNAPII/CDK1 from experiments as in (A) (n = 5). p values were determined by the two-tailed Student's one-sample t test.

(C) Distribution of RNAPII and pRNAPII S5 levels on chromatin in G1 cells 48 h after transfection with scr, siPNUTS, siWDR82#3, and siSSU72 with and without THZ1 and MG132 (4 h).

(D) Mean fold changes from (C) of RNAPII on chromatin in THZ1-treated relative to nontreated cells with and without MG132 in G1 phase (n = 3, except for siSSU72, where n = 2).

(E) As in (D) but showing fold changes of pRNAPII S5.

(F) Effect of MG132 on fold changes after THZ1, as determined by the fold change with MG132 divided by the fold change without MG132 from (D) and (E). If this value is above 1, then MG132 stabilizes pRNAPII S5 and/or RNAPII on chromatin. Data are presented as mean ± SEM (n = 3, except for siSSU72, where n = 2).

(G) As in (F) but in S phase.

p values in (D)–(G) were determined by the two-tailed Student's one-sample t test. Error bars represent SEM.

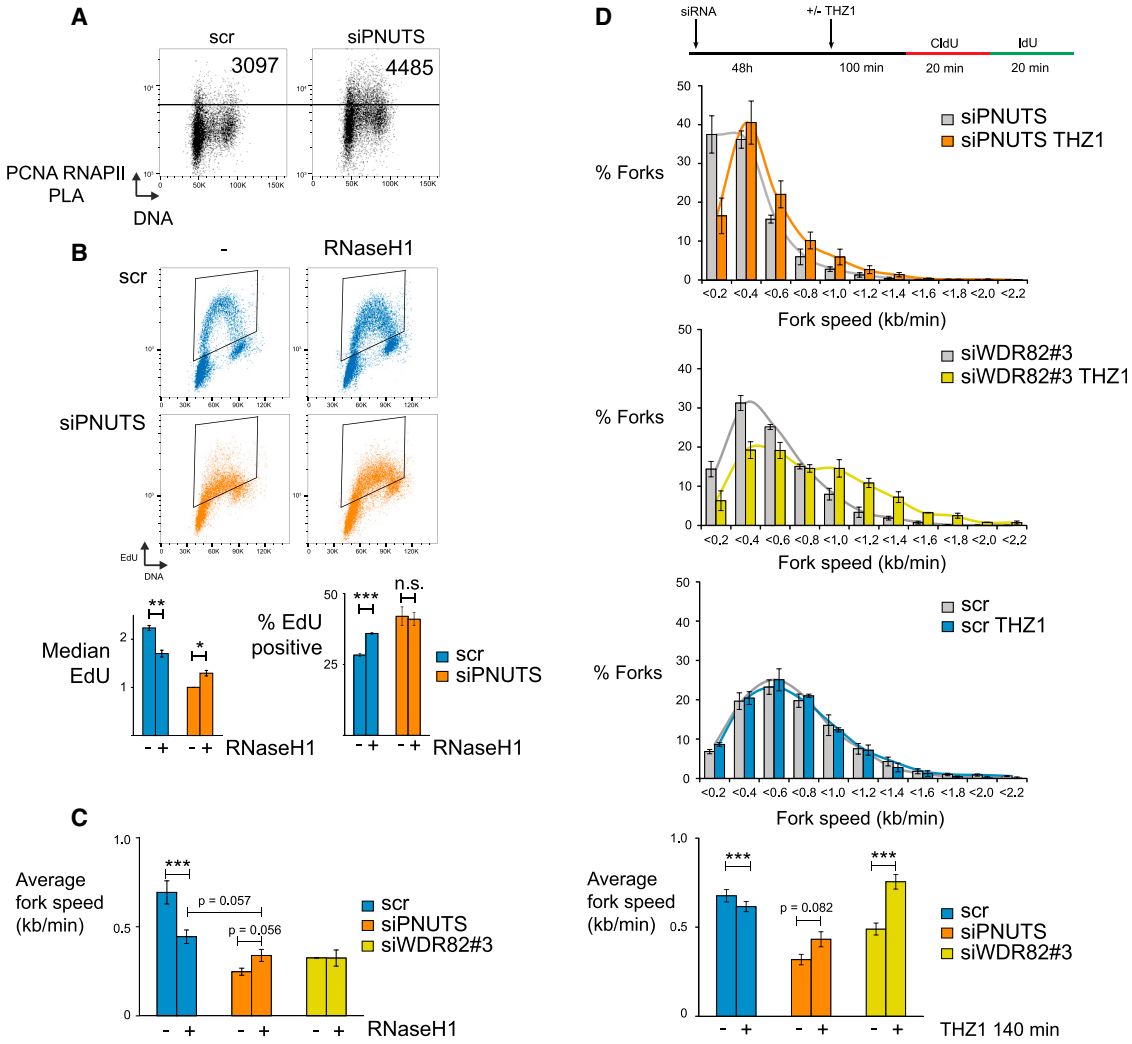

E

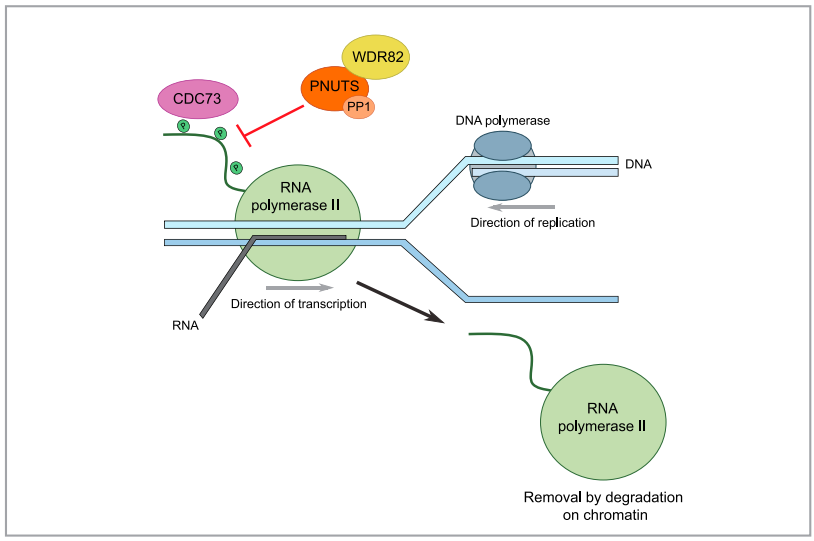

(legend on next page)

roles in RNAPII CTD dephosphorylation. By using a PP1 binding deficient mutant of PNUTS, we show that PP1 is required for the effects of PNUTS on DNA replication and RNAPII residence time (Figures 1E, 1F, 4J, and 4K). Furthermore, depletion of SSU72, a different RNAPII S5 phosphatase, gave similar effects as depletion of PNUTS and WDR82 on DNA replication and RNAPII chromatin stability (Figures 1G, 1H, and 6C–6G), strongly supporting that RNAPII S5 is the relevant substrate for WDR82/PNUTS-PP1. In line with this, co-depletion of the phospho-CTD binding protein CDC73 (Qiu et al., 2012) with PNUTS, suppressed the effects on RNAPII chromatin binding and DNA replication (Figures 5, S5A–S5E, and S5G). Moreover, addition of a transcription inhibitor that prevents *de novo* RNAPII initiation or overexpression of RNaseH1 to remove R-loops partially reversed the replication stress phenotype (Figures 7B–7D). Interestingly, low expression of WDR82 was associated with poor prognosis in colorectal cancer (Liu et al., 2018), but the underlying molecular explanation was unknown. Furthermore, high expression of WDR82 correlated with higher survival in pancreatic cancer, and high expression of PNUTS is a favorable prognostic marker in pancreatic and cervical cancer (Gendoo et al., 2019; Hu et al., 2018; Uhlen et al., 2017). Replication stress is frequently found in pancreatic and colorectal cancers (Manic et al., 2018; Wallez et al., 2018) and can also be induced by human papillomavirus infection, the main cause of cervical cancer (Moody, 2019). Therefore, in light of our results, we propose that PNUTS and WDR82 may prevent tumor aggressiveness by suppressing replication stress.

STAR★METHODS

Detailed methods are provided in the online version of this paper and include the following:

- KEY RESOURCES TABLE
- RESOURCE AVAILABILITY
  - Lead Contact
  - Materials Availability
  - Data and Code Availability
- EXPERIMENTAL MODEL AND SUBJECT DETAILS
- METHOD DETAILS
  - Chemicals and treatments
  - siRNA and DNA transfections
  - Western blotting and antibodies
  - Flow cytometry analysis
  - Chromatin fractionation for western blotting
  - Chromatin fractionation for flow cytometry
  - Proximity ligation assay for flow cytometry
  - Proximity ligation assay by microscopy
  - DNA Fiber assay
  - GFP pulldowns and SILAC experiment
  - Mass spectrometry and data analysis
  - Phosphatase assay
  - Live cell imaging
  - Immunofluorescence
  - Clonogenic survival assay
  - Prognostic data
- QUANTIFICATION AND STATISTICAL ANALYSIS

SUPPLEMENTAL INFORMATION

Supplemental Information can be found online at https://doi.org/10.1016/j.celrep.2020.108469.

ACKNOWLEDGMENTS

We thank the Flow Cytometry Core Facility and Core Facility for Advanced Light Microscopy at the Oslo University Hospital for helpful assistance and Beata Grallert for generating the CDC73 siRNA-resistant cell line. We are grateful for funds from the Norwegian Research Council (275918), the South-Eastern Norway Regional Health Authority (2014035 and 2013017), and the Norwegian Cancer Society (3367910).

AUTHOR CONTRIBUTIONS

H.B.L., L.E.S., and L.T.E.B. conducted most of the experiments. L.T.-M. performed SILAC mass spectrometry (MS) proteomics. B.S. and J.A.M. performed FRAP analysis. C.C. and L.E.S. constructed cells stably expressing siRNA-resistant WDR82. E.P. provided the DNA fiber assay technique and gave expert advice. O.J.B.L. performed initial experiments regarding WDR82. L.E.S., L.T.E.B., L.T.-M., B.S., J.A.M., H.B.L., and R.G.S. planned experiments and analyzed results. H.B.L. and R.G.S. conceived and supervised the study and wrote most of the paper. All authors contributed to editing the manuscript text.

DECLARATIONS OF INTEREST

The authors declare no competing interests.

Received: May 1, 2020
Revised: October 5, 2020
Accepted: November 10, 2020
Published: December 1, 2020

Figure 7. Replication-Transcription Collisions Suppress DNA Replication after Depletion of PNUTS or WDR82

(A) Flow cytometry proximity ligation assay (PLA) analysis showing proximity of RNAPII and PCNA in HeLa cells 72 h after siRNA transfection with scr or siPNUTS. Values in flow cytometry scatterplots show median PLA levels in S phase cells (within the region shown in Figure S6B). The black line is used to ease visual interpretation, as more dots (single cells) are above this line in PNUTS siRNA transfected cells than in control siRNA transfected cells.

(B) Flow cytometry analysis showing EdU incorporation 72 h after transfection with siPNUTS or scr and 48 h after transfection with EGFP-RNaseH1. Samples were stained and analyzed as in Figure 1A. Mean median EdU incorporation and percentage of cells in S phase are shown. (n = 3).

(C) Average replication fork speed from DNA fiber analysis in HeLa cells 48 h after transfection with scr, siPNUTS, or siWDR82#3 and 24 h after transfection with EGFP-RNase H1. p values were determined by the two-tailed Student's one-sample t test.

(D) DNA fiber analysis in HeLa cells at 48 h after siRNA transfection. THZ1 was added for 100 min before and during DNA fiber labeling (total 140 min). Mean replication fork speed and distributions of replication fork speed are shown (n = 3). p values were determined by the two-tailed Student's one-sample t test.

(E) Model for how WDR82/PNUTS-PP1 counteracts T-R collisions. Under regular conditions, WDR82/PNUTS-PP1 contributes to turnover of RNAPII on chromatin by dephosphorylating pRNAPII S5 in a timely manner, thus allowing RNAPII degradation and removal and preventing T-R conflicts. After depletion of PNUTS/WDR82, CDC73 binds to phosphorylated RNAPII and prevents RNAPII degradation, thus creating T-R conflicts. See main text for details.

Error bars represent SEM. See also Figure S6.

REFERENCES

Ahn, S.H., Kim, M., and Buratowski, S. (2004). Phosphorylation of serine 2 within the RNA polymerase II C-terminal domain couples transcription and 3′ end processing. Mol. Cell *13*, 67–76.

Andersen, J.S., Lyon, C.E., Fox, A.H., Leung, A.K., Lam, Y.W., Steen, H., Mann, M., and Lamond, A.I. (2002). Directed proteomic analysis of the human nucleolus. Curr. Biol. *12*, 1–11.

Austenaa, L.M., Barozzi, I., Simonatto, M., Masella, S., Della Chiara, G., Ghisletti, S., Curina, A., de Wit, E., Bouwman, B.A., de Pretis, S., et al. (2015). Transcription of mammalian cis-regulatory elements is restrained by actively enforced early termination. Mol. Cell *60*, 460–474.

Bentley, D.L. (2014). Coupling mRNA processing with transcription in time and space. Nat. Rev. Genet. *15*, 163–175.

Beullens, M., Stalmans, W., and Bollen, M. (1998). The biochemical identification and characterization of new species of protein phosphatase 1. Methods Mol. Biol. *93*, 145–155.

Bjursell, G., and Reichard, P. (1973). Effects of thymidine on deoxyribonucleoside triphosphate pools and deoxyribonucleic acid synthesis in Chinese hamster ovary cells. J. Biol. Chem. *248*, 3904–3909.

Boens, S., Szekér, K., Van Eynde, A., and Bollen, M. (2013). Interactor-guided dephosphorylation by protein phosphatase-1. Methods Mol. Biol. *1053*, 271–281.

Campeau, E., Ruhl, V.E., Rodier, F., Smith, C.L., Rahmberg, B.L., Fuss, J.O., Campisi, J., Yaswen, P., Cooper, P.K., and Kaufman, P.D. (2009). A versatile viral system for expression and depletion of proteins in mammalian cells. PLoS ONE *4*, e6529.

Chakraborty, P., Huang, J.T.J., and Hiom, K. (2018). DHX9 helicase promotes R-loop formation in cells with impaired RNA splicing. Nat. Commun. *9*, 4346.

Ciurciu, A., Duncalf, L., Jonchere, V., Lansdale, N., Vasieva, O., Glenday, P., Rudenko, A., Vissi, E., Cobbe, N., Alphey, L., and Bennett, D. (2013). PNUTS/PP1 regulates RNAPII-mediated gene expression and is necessary for developmental growth. PLoS Genet. *9*, e1003885.

Cortazar, M.A., Sheridan, R.M., Erickson, B., Fong, N., Glover-Cutter, K., Brannan, K., and Bentley, D.L. (2019). Control of RNA Pol II speed by PNUTS-PP1 and Spt5 dephosphorylation facilitates termination by a "sitting duck torpedo" mechanism. Mol. Cell *76*, 896–908.e4.

Custódio, N., and Carmo-Fonseca, M. (2016). Co-transcriptional splicing and the CTD code. Crit. Rev. Biochem. Mol. Biol. *51*, 395–411.

Dull, T., Zufferey, R., Kelly, M., Mandel, R.J., Nguyen, M., Trono, D., and Naldini, L. (1998). A third-generation lentivirus vector with a conditional packaging system. J. Virol. *72*, 8463–8471.

Felipe-Abrio, I., Lafuente-Barquero, J., García-Rubio, M.L., and Aguilera, A. (2015). RNA polymerase II contributes to preventing transcription-mediated replication fork stalls. EMBO J. *34*, 236–250.

Fokas, E., Prevo, R., Pollard, J.R., Reaper, P.M., Charlton, P.A., Cornelissen, B., Vallis, K.A., Hammond, E.M., Olcina, M.M., Gillies McKenna, W., et al. (2012). Targeting ATR in vivo using the novel inhibitor VE-822 results in selective sensitization of pancreatic tumors to radiation. Cell Death Dis. *3*, e441.

Forment, J.V., and O'Connor, M.J. (2018). Targeting the replication stress response in cancer. Pharmacol. Ther. *188*, 155–167.

Gaillard, H., and Aguilera, A. (2016). Transcription as a threat to genome integrity. Annu. Rev. Biochem. *85*, 291–317.

Gaillard, H., García-Muse, T., and Aguilera, A. (2015). Replication stress and cancer. Nat. Rev. Cancer *15*, 276–289.

Gendoo, D.M.A., Zon, M., Sandhu, V., Manem, V.S.K., Ratanasirigulchai, N., Chen, G.M., Waldron, L., and Haibe-Kains, B. (2019). MetaGxData: clinically annotated breast, ovarian and pancreatic cancer datasets and their use in generating a multi-cancer gene signature. Sci. Rep. *9*, 8770.

Gómez-González, B., and Aguilera, A. (2019). Transcription-mediated replication hindrance: a major driver of genome instability. Genes Dev. *33*, 1008–1026.

Hahn, M.A., Dickson, K.A., Jackson, S., Clarkson, A., Gill, A.J., and Marsh, D.J. (2012). The tumor suppressor CDC73 interacts with the ring finger proteins RNF20 and RNF40 and is required for the maintenance of histone 2B monoubiquitination. Hum. Mol. Genet. *21*, 559–568.

Håland, T.W., Boye, E., Stokke, T., Grallert, B., and Syljuåsen, R.G. (2015). Simultaneous measurement of passage through the restriction point and MCM loading in single cells. Nucleic Acids Res. *43*, e150.

Hamperl, S., Bocek, M.J., Saldivar, J.C., Swigut, T., and Cimprich, K.A. (2017). Transcription-replication conflict orientation modulates R-loop levels and activates distinct DNA damage responses. Cell *170*, 774–786.e719.

Harlen, K.M., and Churchman, L.S. (2017). The code and beyond: transcription regulation by the RNA polymerase II carboxy-terminal domain. Nat. Rev. *18*, 263–273.

Hawkins, M., Dimude, J.U., Howard, J.A.L., Smith, A.J., Dillingham, M.S., Savery, N.J., Rudolph, C.J., and McGlynn, P. (2019). Direct removal of RNA polymerase barriers to replication by accessory replicative helicases. Nucleic Acids Res. *47*, 5100–5113.

Hein, M.Y., Hubner, N.C., Poser, I., Cox, J., Nagaraj, N., Toyoda, Y., Gak, I.A., Weisswange, I., Mansfeld, J., Buchholz, F., et al. (2015). A human interactome in three quantitative dimensions organized by stoichiometries and abundances. Cell *163*, 712–723.

Hodroj, D., Recolin, B., Serhal, K., Martinez, S., Tsanov, N., Abou Merhi, R., and Maiorano, D. (2017). An ATR-dependent function for the Ddx19 RNA helicase in nuclear R-loop metabolism. EMBO J. *36*, 1182–1198.

Hu, D., Ansari, D., Pawłowski, K., Zhou, Q., Sasor, A., Welinder, C., Kristl, T., Bauden, M., Rezeli, M., Jiang, Y., et al. (2018). Proteomic analyses identify prognostic biomarkers for pancreatic ductal adenocarcinoma. Oncotarget *9*, 9789–9807.

Jackson, D.A., and Pombo, A. (1998). Replicon clusters are stable units of chromosome structure: evidence that nuclear organization contributes to the efficient activation and propagation of S phase in human cells. J. Cell Biol. *140*, 1285–1295.

Jensen, T.H., Jacquier, A., and Libri, D. (2013). Dealing with pervasive transcription. Mol. Cell *52*, 473–484.

Jones, R.M., Mortusewicz, O., Afzal, I., Lorvellec, M., García, P., Helleday, T., and Petermann, E. (2013). Increased replication initiation and conflicts with transcription underlie Cyclin E-induced replication stress. Oncogene *32*, 3744–3753.

Klusmann, I., Wohlberedt, K., Magerhans, A., Teloni, F., Korbel, J.O., Altmeyer, M., and Dobbelstein, M. (2018). Chromatin modifiers Mdm2 and RNF2 prevent RNA:DNA hybrids that impair DNA replication. Proc. Natl. Acad. Sci. USA *115*, E11311–E11320.

Kotsantis, P., Silva, L.M., Irmscher, S., Jones, R.M., Folkes, L., Gromak, N., and Petermann, E. (2016). Increased global transcription activity as a mechanism of replication stress in cancer. Nat. Commun. *7*, 13087.

Kreivi, J.P., Trinkle-Mulcahy, L., Lyon, C.E., Morrice, N.A., Cohen, P., and Lamond, A.I. (1997). Purification and characterisation of p99, a nuclear modulator of protein phosphatase 1 activity. FEBS Lett. *420*, 57–62.

Krishnamurthy, S., He, X., Reyes-Reyes, M., Moore, C., and Hampsey, M. (2004). Ssu72 Is an RNA polymerase II CTD phosphatase. Mol. Cell *14*, 387–394.

Kwiatkowski, N., Zhang, T., Rahl, P.B., Abraham, B.J., Reddy, J., Ficarro, S.B., Dastur, A., Amzallag, A., Ramaswamy, S., Tesar, B., et al. (2014). Targeting transcription regulation in cancer with a covalent CDK7 inhibitor. Nature *511*, 616–620.

Landsverk, H.B., Mora-Bermúdez, F., Landsverk, O.J., Hasvold, G., Naderi, S., Bakke, O., Ellenberg, J., Collas, P., Syljuåsen, R.G., and Küntziger, T. (2010). The protein phosphatase 1 regulator PNUTS is a new component of the DNA damage response. EMBO Rep. *11*, 868–875.

Landsverk, H.B., Sandquist, L.E., Sridhara, S.C., Rødland, G.E., Sabino, J.C., de Almeida, S.F., Grallert, B., Trinkle-Mulcahy, L., and Syljuåsen, R.G. (2019). Regulation of ATR activity via the RNA polymerase II associated factors CDC73 and PNUTS-PP1. Nucleic Acids Res. *47*, 1797–1813.

Lang, K.S., Hall, A.N., Merrikh, C.N., Ragheb, M., Tabakh, H., Pollock, A.J., Woodward, J.J., Dreifus, J.E., and Merrikh, H. (2017). Replication-transcription conflicts generate R-loops that orchestrate bacterial stress survival and pathogenesis. Cell *170*, 787–799.e18.

Lee, J.H., and Skalnik, D.G. (2008). Wdr82 is a C-terminal domain-binding protein that recruits the Setd1A Histone H3-Lys4 methyltransferase complex to transcription start sites of transcribed human genes. Mol. Cell. Biol. *28*, 609–618.

Lee, J.H., You, J., Dobrota, E., and Skalnik, D.G. (2010). Identification and characterization of a novel human PP1 phosphatase complex. J. Biol. Chem. *285*, 24466–24476.

Liu, B., and Alberts, B.M. (1995). Head-on collision between a DNA replication apparatus and RNA polymerase transcription complex. Science *267*, 1131–1137.

Liu, H., Li, Y., Li, J., Liu, Y., and Cui, B. (2018). H3K4me3 and Wdr82 are associated with tumor progression and a favorable prognosis in human colorectal cancer. Oncol. Lett. *16*, 2125–2134.

Manic, G., Signore, M., Sistigu, A., Russo, G., Corradi, F., Siteni, S., Musella, M., Vitale, S., De Angelis, M.L., Pallocca, M., et al. (2018). CHK1-targeted therapy to deplete DNA replication-stressed, p53-deficient, hyperdiploid colorectal cancer stem cells. Gut *67*, 903–917.

McKay, B.C., Chen, F., Clarke, S.T., Wiggin, H.E., Harley, L.M., and Ljungman, M. (2001). UV light-induced degradation of RNA polymerase II is dependent on the Cockayne's syndrome A and B proteins but not p53 or MLH1. Mutat. Res. *485*, 93–105.

Moody, C.A. (2019). Impact of replication stress in human papillomavirus pathogenesis. J. Virol. *93*, e01012–e01017.

Mortensen, P., Gouw, J.W., Olsen, J.V., Ong, S.E., Rigbolt, K.T., Bunkenborg, J., Cox, J., Foster, L.J., Heck, A.J., Blagoev, B., et al. (2010). MSQuant, an open source platform for mass spectrometry-based quantitative proteomics. J. Proteome Res. *9*, 393–403.

Nojima, T., Gomes, T., Grosso, A.R.F., Kimura, H., Dye, M.J., Dhir, S., Carmo-Fonseca, M., and Proudfoot, N.J. (2015). Mammalian NET-seq reveals genome-wide nascent transcription coupled to RNA processing. Cell *161*, 526–540.

Poli, J., Gerhold, C.B., Tosi, A., Hustedt, N., Seeber, A., Sack, R., Herzog, F., Pasero, P., Shimada, K., Hopfner, K.P., and Gasser, S.M. (2016). Mec1, INO80, and the PAF1 complex cooperate to limit transcription replication conflicts through RNAPII removal during replication stress. Genes Dev. *30*, 337–354.

Pomerantz, R.T., and O'Donnell, M. (2010). Direct restart of a replication fork stalled by a head-on RNA polymerase. Science *327*, 590–592.

Prévost, M., Chamousset, D., Nasa, I., Freele, E., Morrice, N., Moorhead, G., and Trinkle-Mulcahy, L. (2013). Quantitative fragmentome mapping reveals novel, domain-specific partners for the modular protein RepoMan (recruits PP1 onto mitotic chromatin at anaphase). Mol. Cell. Proteomics *12*, 1468–1486.

Qiu, H., Hu, C., Gaur, N.A., and Hinnebusch, A.G. (2012). Pol II CTD kinases Bur1 and Kin28 promote Spt5 CTR-independent recruitment of Paf1 complex. EMBO J. *31*, 3494–3505.

Rockx, D.A., Mason, R., van Hoffen, A., Barton, M.C., Citterio, E., Bregman, D.B., van Zeeland, A.A., Vrieling, H., and Mullenders, L.H. (2000). UV-induced inhibition of transcription involves repression of transcription initiation and phosphorylation of RNA polymerase II. Proc. Natl. Acad. Sci. USA *97*, 10503–10508.

Santos-Pereira, J.M., and Aguilera, A. (2015). R loops: new modulators of genome dynamics and function. Nat. Rev. Genet. *16*, 583–597.

Schneider, C.A., Rasband, W.S., and Eliceiri, K.W. (2012). NIH Image to ImageJ: 25 years of image analysis. Nat. Methods *9*, 671–675.

Sirbu, B.M., McDonald, W.H., Dungrawala, H., Badu-Nkansah, A., Kavanaugh, G.M., Chen, Y., Tabb, D.L., and Cortez, D. (2013). Identification of proteins at active, stalled, and collapsed replication forks using isolation of proteins on nascent DNA (iPOND) coupled with mass spectrometry. J. Biol. Chem. *288*, 31458–31467.

Somesh, B.P., Reid, J., Liu, W.F., Søgaard, T.M., Erdjument-Bromage, H., Tempst, P., and Svejstrup, J.Q. (2005). Multiple mechanisms confining RNA polymerase II ubiquitylation to polymerases undergoing transcriptional arrest. Cell *121*, 913–923.

Sørensen, C.S., and Syljuåsen, R.G. (2012). Safeguarding genome integrity: the checkpoint kinases ATR, CHK1 and WEE1 restrain CDK activity during normal DNA replication. Nucleic Acids Res. *40*, 477–486.

Steurer, B., Janssens, R.C., Geverts, B., Geijer, M.E., Wienholz, F., Theil, A.F., Chang, J., Dealy, S., Pothof, J., van Cappellen, W.A., et al. (2018). Live-cell analysis of endogenous GFP-RPB1 uncovers rapid turnover of initiating and promoter-paused RNA polymerase II. Proc. Natl. Acad. Sci. USA *115*, E4368–E4376.

Stork, C.T., Bocek, M., Crossley, M.P., Sollier, J., Sanz, L.A., Chédin, F., Swigut, T., and Cimprich, K.A. (2016). Co-transcriptional R-loops are the main cause of estrogen-induced DNA damage. eLife *5*, e17548.

Swingle, M., Ni, L., and Honkanen, R.E. (2007). Small-molecule inhibitors of ser/thr protein phosphatases: specificity, use and common forms of abuse. Methods Mol. Biol. *365*, 23–38.

Timson, J. (1975). Hydroxyurea. Mutat. Res. *32*, 115–132.

Trinkle-Mulcahy, L. (2012). Resolving protein interactions and complexes by affinity purification followed by label-based quantitative mass spectrometry. Proteomics *12*, 1623–1638.

Trinkle-Mulcahy, L., Ajuh, P., Prescott, A., Claverie-Martin, F., Cohen, S., Lamond, A.I., and Cohen, P. (1999). Nuclear organisation of NIPP1, a regulatory subunit of protein phosphatase 1 that associates with pre-mRNA splicing factors. J. Cell Sci. *112*, 157–168.

Trinkle-Mulcahy, L., Andersen, J., Lam, Y.W., Moorhead, G., Mann, M., and Lamond, A.I. (2006). Repo-Man recruits PP1 gamma to chromatin and is essential for cell viability. J. Cell Biol. *172*, 679–692.

Uhlen, M., Zhang, C., Lee, S., Sjöstedt, E., Fagerberg, L., Bidkhori, G., Benfeitas, R., Arif, M., Liu, Z., Edfors, F., et al. (2017). A pathology atlas of the human cancer transcriptome. Science *357*, eaan2507.

Verheyen, T., Görnemann, J., Verbinnen, I., Boens, S., Beullens, M., Van Eynde, A., and Bollen, M. (2015). Genome-wide promoter binding profiling of protein phosphatase-1 and its major nuclear targeting subunits. Nucleic Acids Res. *43*, 5771–5784.

Wallez, Y., Dunlop, C.R., Johnson, T.I., Koh, S.B., Fornari, C., Yates, J.W.T., Bernaldo de Quirós Fernández, S., Lau, A., Richards, F.M., and Jodrell, D.I. (2018). The ATR inhibitor AZD6738 synergizes with gemcitabine *in vitro* and *in vivo* to induce pancreatic ductal adenocarcinoma regression. Mol. Cancer Ther. *17*, 1670–1682.

Winsor, T.S., Bartkowiak, B., Bennett, C.B., and Greenleaf, A.L. (2013). A DNA damage response system associated with the phosphoCTD of elongating RNA polymerase II. PLoS ONE *8*, e60909.

Wu, D., De Wever, V., Derua, R., Winkler, C., Beullens, M., Van Eynde, A., and Bollen, M. (2018). A substrate-trapping strategy for protein phosphatase PP1 holoenzymes using hypoactive subunit fusions. J. Biol. Chem. *293*, 15152–15162.

Yasukawa, T., Kamura, T., Kitajima, S., Conaway, R.C., Conaway, J.W., and Aso, T. (2008). Mammalian Elongin A complex mediates DNA-damage-induced ubiquitylation and degradation of Rpb1. EMBO J. *27*, 3256–3266.

STAR★METHODS

KEY RESOURCES TABLE

REAGENT or RESOURCE	SOURCE	IDENTIFIER
Antibodies		
CDC73 (Lot #2)	Bethyl Laboratories	Cat#A300-170A; RRID:AB_309449
CDK1 (Clone 17)	Santa Cruz Biotechnology	Cat#sc-54; RRID:AB_627224
CHK1 (Clone DCS-310)	Santa Cruz Biotechnology	Cat#sc-56291; RRID:AB_1121554
CldU (rat anti-bromodeoxyuridine) (Clone BU1/75 (ICR1))	Abcam	Cat#ab74545; RRID:AB_1523224
CldU and IdU (mouse anti-bromodeoxuridine) (Clone B44)	BD Biosciences	Cat#B44; RRID:AB_2313824
GFP (Clones 7.1 and 13.1)	Sigma Aldrich	Cat#11814460001; RRID:AB_390913
γH2AX (Clone jbw301)	Millipore	Cat#05-636; RRID:AB_309864
γTUBULIN (Clone GTU-88)	Sigma Aldrich	Cat#T6557; RRID:AB_477584
LAMIN B (Clone D8P3U)	Cell Signaling Technology	Cat#12255; RRID:AB_2797859
MCM7 (Clone DCS-141)	Santa Cruz Biotechnology	Cat#sc-65469; RRID:AB_1125698
PCNA (Lot #GR3240364-1)	Abcam	Cat#ab18197; RRID:AB_444313
phosphoCHK1 S317 (Lot #12)	Cell Signaling Technology	Cat#2344; RRID:AB_331488
phosphoCHK1 S345 (Lot #18)	Cell Signaling Technology	Cat#2341; RRID:AB_330023
phosphoRNAPII S2 (Clone 3E10)	Millipore	Cat#04-1571; RRID:AB_10627998
phosphoRNAPII S5 (Clone 3E8)	Millipore	Cat#04-1572; RRID:AB_11213421
phosphoRPA32 S33 (Lot #7)	Bethyl Laboratories	Cat#A300-246A; RRID:AB_2180847
phosphoRPA32 S4S8 (Lot #6)	Bethyl Laboratories	A300-245A; RRID:AB_210547
PNUTS (Clone 47)	BD Biosciences	Cat#611060; RRID:AB_398373
PP1γ (Clone C-19)	Santa Cruz Biotechnology	Cat#sc-6108; RRID:AB_2168091
RNAPII C terminus (Clone 1PB-7C2)	Proteogenics	Cat#PTGX-PB-7C2; RRID:AB_2847823
RNAPII N terminus (Clone D8L4Y)	Cell Signaling Technology	Cat#14958; RRID:AB_2687876
RNAPII N terminus (Clone F-12)	Santa Cruz Biotechnology	Cat#sc-55492; RRID:AB_630203
RPA70 (Lot #3)	Cell Signaling Technology	Cat#2267; RRID:AB_2180506
TOX4 (Lot #G1915)	Santa Cruz Biotechnology	Cat#sc-102139; RRID:AB_2206288
WDR82 (Clone D2I3B)	Cell Signaling Technology	Cat#99715; RRID:AB_2800319
WDR82 (Lot #A1212)	Santa Cruz Biotechnology	Cat#sc-103325; RRID:AB_10838774
Chemicals, Peptides, and Recombinant Proteins		
Thymidine	Sigma Aldrich	CAS: 50-89-5
Hydroxyurea	Sigma Aldrich	CAS: 127-07-1
5-Chloro-2′-deoxyuridine	Sigma Aldrich	CAS: 50-90-8
5-Iodo-2′-deoxyuridine	Sigma Aldrich	CAS: 54-42-2
GFP-Trap_Dynabeads	Chromotek	Cat#gtm-20
Complete EDTA-free Protease Inhibitor Cocktail	Merck	Cat#5892791001
PhosSTOP phosphatase inhibitors	Merck	Cat#4906837001
Benzonase	Merck	Cat#70664-3
Calyculin A	Sigma Aldrich	CAS: 101932-71-2
THZ1	ApexBio	CAS: 1604810-83-4
EdU	Thermo Fisher	CAS: 61135-33-9
Pacific Blue Succinimidyl Ester	Thermo Fisher	CAS: 215868-33-0
Alexa Fluor 647 NHS Ester (Succinimidyl Ester)	Thermo Fisher	Cat#A20006

(*Continued on next page*)

Continued

REAGENT or RESOURCE	SOURCE	IDENTIFIER
Formalin solution	Sigma Aldrich	Cat#HT5011
VE822	Selleckchem	CAS: 1232416-25-9
MG132	Sigma Aldrich	CAS: 133407-82-6
Critical Commercial Assays		
Click-iT Plus EdU Alexa Fluor 594 Flow Cytometry Assay Kit	Thermo Fisher	Cat#C10646
Click-iT Plus EdU Alexa Fluor 488 Flow Cytometry Assay Kit	Thermo Fisher	Cat#C10633
Duolink flowPLA Detection Kit - Orange	Sigma Aldrich	Cat#DUO94003
Duolink *In Situ* Detection Reagents Red	Sigma Aldrich	Cat#DUO92008
Duolink *In Situ* PLA Probe Anti-Mouse MINUS	Sigma Aldrich	Cat#DUO92004
Duolink *In Situ* PLA Probe Anti-Mouse PLUS	Sigma Aldrich	Cat#DUO92002
Experimental Models: Cell Lines		
HeLa (human female adenocarcinoma epithelial cells)	Landsverk et al., 2019	N/A
U2OS (human female osteosarcoma epithelial cells)	Landsverk et al., 2019	N/A
GFP- POLR2A knockin MRC5 SV40 cells (Human male fetal lung, SV40 transformed fibroblast cells)	Steurer et al., 2018	N/A
HeLa GFP mpnuts (HeLa BAC clones stably expressing GFP mouse pnuts)	Hyman laboratory	N/A
HeLa CDC73-res cells (HeLa cells stably expressing siRNA resistant untagged wildtype CDC73)	This paper	N/A
HeLa WDR82-res cells (HeLa cells stably expressing siRNA resistant unagged wildtype WDR82)	This paper	N/A
Oligonucleotides		
Scr (scrambled control siRNA) GGUUUCUGUCAAAUGCAAACGGCUU	Landsverk et al., 2010	Stealth siRNA
siRNA targeting sequence: PNUTS (siPNUTS) GCAAUAGUCAGGAGCGAUA	Thermo Fisher (Landsverk et al., 2019)	Silencer select s328
siCDC73 AAACAAGGUUGUCAACGAGAA	Hahn et al., 2012	N/A
siRNA targeting sequence: WDR82 (siWDR82 #1) CUACCUUUAAGAUGCAGUA	Sigma-Aldrich	SASI_Hs02_00358014
siRNA targeting sequence: WDR82 (siWDR82 #2) CCUUUAAGAUGCAGUAUGA	Sigma-Aldrich	SASI_Hs02_00358015
siRNA targeting sequence: WDR82 (siWDR82 #3) CAAAAUAGACGAUACUAUU	Thermo Fisher	Silencer select s58697
siRNA targeting sequence: SSU72 (siSSU72) GGAGCUUCCUGUUGUUCAU	Sigma-Aldrich (Landsverk et al., 2019)	SASI_Hs01_00024012
Recombinant DNA		
pEGFP PNUTS	Landsverk et al., 2019	N/A
pEGFP PNUTS (V399A, W401A)	Landsverk et al., 2019	N/A
pEGFP-RNaseH1	Landsverk et al., 2019	N/A
pPNUTS EGFP	Landsverk et al., 2010	N/A

(*Continued on next page*)

Continued

REAGENT or RESOURCE	SOURCE	IDENTIFIER
pEGFP WDR82	This paper	N/A
pEGFP TOX4	This paper	N/A
Software and Algorithms		
ImageJ	Schneider et al., 2012	https://imagej.nih.gov/ij/
FlowJo 10.6.0	BD Biosciences	N/A
Image Lab	BioRad	N/A
MS-Quant	Mortensen et al., 2010	http://msquant.sourceforge.net
Axiovision 4.8.2	Carl Zeiss	N/A
FACS Diva	BD Biosciences	N/A

RESOURCE AVAILABILITY

Lead Contact

Further information and requests for resources and reagents should be directed to and will be fulfilled by the Lead Contact, Randi Syljuåsen (randi.syljuasen@rr-research.no).

Materials Availability

All reagents generated in this study are available upon request to the Lead Contact.

Data and Code Availability

The published article includes all datasets generated or analyzed during this study (Table S1).

EXPERIMENTAL MODEL AND SUBJECT DETAILS

Human female cervical cancer HeLa Kyoto and female osteosarcoma U2OS cells were grown at 37°C in Dulbecco's modified Eagle's medium (DMEM) and human male SV40 transformed fetal lung fibroblast MRC5 cells were grown in DMEM: Nutrient Mixture F-12 supplemented with antibiotics and 10% fetal bovine serum, at 37°C; 20% O_2, and 5% CO_2 in a humidified incubator. Throughout the manuscript, HeLa Kyoto (HeLa) cells were used unless otherwise stated. The cell lines, with exception of the MRC5 cells, were authenticated by short tandem repeat profiling using Powerplex 16 (Promega) and regularly tested for mycoplasma contamination. HeLa BAC cells stably expressing EGFP mouse pnuts were a generous gift from the laboratory of Tony Hyman. MRC5 cells with knockin GFP POLR2A (Referred to in text as GFP RNAPII) were previously described (Steurer et al., 2018). To generate the untagged CDC73-res cell lines, siRNA resistant CDC73 was cloned as previously described (Landsverk et al., 2019). HeLa cells were transduced and cells carrying the transgene were selected with 0.5 μg/ml puromycin. For the WDR82-res cell lines, the weak PGK promoter was used for transgene expression to achieve low expression levels. Third generation Lentivirus was generated using procedures and plasmids as previously described (Campeau et al., 2009). Briefly, an untagged siRNA-resistant WDR82 allele was cloned into Gateway ENTRY plasmids using standard molecular biology techniques. From these vectors, Lentiviral transfer vectors were generated by recombination into lentiviral destination vectors (vectors derived from Addgene plasmid #19068 and pCDH-EF1α-MCS-IRES-PURO (SystemBiosciences, inc.)) using Gateway LR reactions. VSV-G pseudotyped lentiviral particles were packaged using a third generation packaging system (Dull et al., 1998) (Addgene plasmids # 12251, 12253, 12259). HeLa Kyoto cells were then transduced with low virus titers (MOI $\leq$ 1) and stable expressing populations were generated by antibiotic selection.

METHOD DETAILS

Chemicals and treatments

Thymidine (Sigma Aldrich) was used at 2 mM, Hydroxyurea (Sigma Aldrich) at 100 μM, CDK7-inhibitor THZ1 (ApexBio) at 1 μM, EdU (Thermo Fisher) at 2 μM, VE822 (Selleckchem) at 500 nM and MG132 (Sigma Aldrich) at 50 μM. Note that thymidine, like hydroxyurea (Timson, 1975), suppresses replication by inhibiting deoxyribonucleotide synthesis (Bjursell and Reichard, 1973).

siRNA and DNA transfections

Wild-type and RAXA(V399A,W401A) full-length pEGFP PNUTS, pEGFP RNaseH1 and pEGFP NIPP1 have been previously described (Landsverk et al., 2019; Trinkle-Mulcahy et al., 1999). For the SILAC IP, PNUTS EGFP lacking the seven C-terminal aminoacids was used (Landsverk et al., 2010). The WDR82 gene was synthesized from geneart and cloned into pEGFP-C1. During gene synthesis, the encoded amino acid sequence was kept constant, but the nucleotide sequence was altered to enhance genesynthesis, resulting in

siRNA resistance against siWDR82#3. TOX4 was ordered from Open Biosystems (*Homo sapiens* MGC verified FL cDNA, Clone ID: 3880134, Accession: BC013689), and cloned into pEGFP-C1 (Clontech), using EcoRI/SalI restriction sites and the following primers: FWD_EcoRI:

GATCGAATTCTATGGAGTTTCCCGGAGGAAATG and REV_SalI:

GATCGTCGACTTTCACAAACACCACTGTGTTTG. Sequences of siRNA oligonucleotides can be found in the Key Resources Table. siRNA was transfected using Oligofectamine or RNAimax (Life technologies), and plasmid DNA with Fugene HD (Promega) or Attractene (QIAGEN). Experiments were performed 65–72 h after siRNA transfection unless otherwise stated.

Western blotting and antibodies

Quantitative western blotting was performed as previously described (Landsverk et al., 2019). Briefly, cells were resuspended in ice-cold TX-100 buffer (100 mM NaCl, 50 mM Tris pH 7.5, 2 mM $MgCl_2$, 0.5% TX-100) containing 100 U/ml Benzonase (Sigma-Aldrich), Complete EDTA-free Protease Inhibitor Cocktail (Merck) and PhosSTOP phosphatase inhibitors (Merck). After 24 h incubation at 4°C, Lane Marker Reducing Sample Buffer (Pierce Biotechnologies) was added and samples were boiled (95°C, 5 min). Criterion TGX gels (BioRad) and nitrocellulose membranes (BioRad) were used for separation and transfer. Antibodies used are found in Key Resources Table. Blots were imaged in a Chemidoc MP (BioRad) using chemiluminescence substrates (Supersignal west pico, dura or femto; Thermo Scientific). Quantifications were performed and images processed in Image Lab 4.1 (BioRad) software. Range of detection was verified by including a dilution series of one of the samples and excluding saturated signals. The resulting standard curve allowed accurate quantification. To blot for total protein after detection of a phosphorylated protein, membranes were stripped using ReBlot Plus Mild Antibody Stripping Solution (Millipore).

Flow cytometry analysis

For analysis of EdU incorporation, cells were labeled for 1 h with 2 μM EdU (Thermo Fisher) and fixed in 70% ethanol or, when GFP fluorescence was simultaneously monitored, formalin solution (Sigma Aldrich). EdU was labeled with the Click-iT Plus EdU Alexa Fluor 488 or 594 Flow Cytometry Assay Kits (Thermo Fisher), and DNA with FxCycle Far Red (Thermo Fisher) or Hoechst 33258 (Thermo Fisher). EdU positive cells (shown in black region in Figure 1A) were defined as S phase cells, and median EdU levels were measured within these. When GFP fluorescence was simultaneously monitored, GFP positive cells were selected prior to further analysis. In most of the flow cytometry experiments, with exception of those involving RPA loading, γH2AX or DNA profiles alone, barcoding was performed as previously described (Håland et al., 2015), using either Pacific blue or Alexa Fluor 647 Succinimidyl Ester, to eliminate variation in antibody/EdU staining between the individual samples. Briefly, samples were incubated with dilutions in the range of 0.001 – 0.1 ng/μL Pacific blue Succinimidyl Ester (Thermo Fisher) or 0,002 μg/μL Alexa Fluor 647 Succinimidyl Ester (Thermo Fisher) in PBS for 30 min prior to staining. The barcoded cells were added to the other cells prior to labeling, thus acting as an internal standard which were separated by gating during analysis. Flow cytometry analysis of γH2AX staining and RPA loading was performed as previously described (Håland et al., 2015; Landsverk et al., 2019). Briefly, for measuring RPA loading, the cells were treated with 750 μL low salt extraction buffer (0.1% Igepal CA-630, 10 mM NaCl, 5 mM $MgCl_2$, 0.1 mM PMSF, 10 mM Potassium phosphate buffer (pH 7.4)) for 5 min on ice, fixed by adding 250 μL formalin (Sigma Aldrich) and incubation was continued for 1 h on ice. For γH2AX labeling, cells were fixed directly in ice cold 70% ethanol. The samples were next incubated with primary (anti-RPA70 or anti-γH2AX) and secondary antibodies (Alexa Flour 488 and 647), diluted in flow buffer (0.1% Igepal CA-630, 6.5 mM Na2HPO4, 1.5 mM KH2PO4, 2.7 mM KCl, 137 mM NaCl, 0.5 mM ethylenediaminetetraacetic acid (pH7.5)) containing 4% non-fat milk, and stained with the DNA-stains Hoechst 33258 or FxCycle. Note that in the rescue experiments with CDC73 (Figure 5H), depletions of CDC73 and PNUTS were verified by western blotting (Figure S5E). Samples were analyzed in a LSRII flow cytometer (BD Biosciences) and processed in FACSDiva and FlowJo software (Both BD Biosciences).

Chromatin fractionation for western blotting

For chromatin fractionation of western blotting samples, cells were harvested, isolated by centrifugation and washed in PBS. To release non-chromatin bound factors, the cell pellet was resuspended in ice-cold chromatin extraction buffer (20 mM HEPES (pH 7.9), 1.5 mM $MgCl_2$, 50 mM NaCl, 300 mM Sucrose, 0.5% TX-100, Complete EDTA-free Protease Inhibitor Cocktail (Merck), PhosSTOP phosphatase inhibitors (Merck) and 20 μM MG132 (Sigma Aldrich)) and incubated for 10 min at 4°C with gentle mixing (300 rpm). Soluble and chromatin bound fractions were separated by centrifugation. The pellet containing chromatin bound factors was washed once in chromatin extraction buffer, followed by chromatin digestion for 2 h at 4°C with gentle mixing (300 rpm) in chromatin extraction buffer containing 100 U/mL Benzonase (Sigma Aldrich). Lane Marker Reducing Sample Buffer (Pierce Biotechnologies) was added to both soluble and chromatin bound fraction samples, and the samples were boiled for 5 min at 95°C prior to analysis by quantitative western blotting. Final volumes of soluble versus chromatin bound fractions were kept equal, so they could be directly compared. Notably, as we included a dilution curve in the western blots after chromatin fractionation, in our study this method was superior for determining absolute values.

Chromatin fractionation for flow cytometry

For flow cytometry analysis of chromatin bound RNAPII, cell pellets were resuspended in 100 μL chromatin extraction buffer for 5 min on ice. The cells were fixed by addition of formalin solution (Sigma Aldrich) directly to the cell suspension at a ratio of 10:1 of formalin

versus chromatin extraction buffer, and incubated at room temperature for 10 min. Cells were then washed once in PBS and barcoded and labeled as above (see γH2AX and RPA staining) with antibodies to RNAPII and pRNAPII S5 with the following modifications. One barcoded (with Pacific blue or Alexa Fluor 647) control sample of non-treated, non-extracted HeLa cells was added to all the individual samples. This provided an internal control both for extraction efficiency and for normalization, resulting in highly accurate quantifications. In addition, a secondary antibody control was included in each experiment, where primary antibody staining was omitted, allowing subtraction of background due to secondary antibody staining. Note that for the experiments involving MG132, the rescue experiments with EGFP PNUTS^{wt} and EGFP PNUTS^{RAXA}, and the experiments with siSSU72, chromatin extraction buffer with 140 mM NaCl was used. The higher NaCl concentration enhanced the differences in RNAPII and pRNAPII S5 chromatin binding between THZ1 treated and non-treated samples. In the rescue experiments with EGFP PNUTS^{wt} and EGFP PNUTS^{RAXA}, efficient knockdown of endogenous PNUTS was verified by western blotting and equal expression of the GFP constructs was verified by GFP expression by flow cytometry (Figures S4G and S4H).

Proximity ligation assay for flow cytometry

The proximity ligation assay (PLA) for flow cytometry (Duolink flowPLA Detection Kit – Orange (Sigma Aldich)) was performed in accordance to the manufacturer's instructions with the following modifications. At 72 h after siRNA transfection, HeLa cells were harvested, counted (8 × 10^5 cells per condition were used per 100 μL Duolink reaction volume) and fixed in 70% ethanol for 24 h or more at −20°C. Next, cells were barcoded with Pacific Blue, mixed and split into different tubes: one stained with both antibodies (anti-PCNA and anti-RNAPII) and both PLA probes, both antibodies and only one PLA probe, only one of the antibodies, but both PLA probes, or unstained (For overview see Figure S6A). Cells were blocked for 5 min in flow buffer (0.1% Igepal CA-630, 6.5 mM Na_2HPO_4, 1.5 mM KH_2PO_4, 2.7 mM KCl, 137 mM NaCl, 0.5 mM EDTA (pH7.5)), containing 4% (w/v) non-fat milk, and incubated with antibodies diluted in blocking buffer at 4°C overnight. After this, cells were washed once with 500 μL PBS with 1% FBS and incubated with pre-mixed PLA probe anti-rabbit minus and PLA probe anti-mouse plus diluted in PLA blocking buffer for 1 h at 37°C. The subsequent steps were carried out in accordance to manufacturer's instructions using 100 min amplification time and 30 min detection time. Finally, the cells were resuspended in PBS containing 1 μl/ml FxCycle Red (Thermo Fisher) and 50 μl/ml Ribonuclease A (QIAGEN). The cells were then analyzed in a LSRII flow cytometer (BD Biosciences) and processed in FACSDiva and FlowJo software (Both BD Biosciences).

Proximity ligation assay by microscopy

For detection of proximity between RNAPII and PCNA using the proximity ligation assay for immunofluoresence microscopy, HeLa cells were pre-extracted in detergent buffer (20 mM HEPES, pH 7.4; 50 mM NaCl; 1.5 mM MgCl2: 300 mM sucrose; 0.05% Triton X-100) for 5 min on ice prior to fixation with formalin. Coverslips were stained with anti-RNAPII (1PB 7C2, Proteogenix) and anti- PCNA (Abcam) in PBS-AT (PBS with 0.5% Triton X-100 and 1% BSA) overnight. The subsequent steps in proximal ligation assay were carried out with Duolink *In Situ* Orange Kit Mouse/Rabbit (Sigma Aldrich) in accordance to manufacturer's instructions (100 min amplification time). Cells were examined with a Zeiss LSM 880 confocal microscope (Carl Zeiss MicroImaging GmbH, Jena, Germany) equipped with an Ar-Laser Multiline (458/488/514 nm), a DPSS-561 10 (561 nm), a Laser diode 405-30 CW (405 nm), and a HeNe-laser (633 nm). The objective used was a Zeiss C-Apochromat 40x NA/1.2 W DICIII.

DNA Fiber assay

HeLa cells were pulse labeled with 25 μM 5-Chloro-2′-deoxyuridine (CldU) (Sigma Aldrich) followed by 250 μM 5-Iodo-2′-deoxyuridine (IdU) (Sigma Aldrich) for 20 min each. After labeling, cells were harvested and resuspended in ice-cold PBS. DNA fiber spreads were prepared by spotting 2 μL of cells (5 × 10^5 cells per mL in PBS) onto microscope slides (SuperFrost, Thermo Scientific), followed by lysis with 7 μL of 0.5% SDS, 200 mM Tris-HCl pH 7.4 and 50 mM EDTA for 5-7 min before spreading. DNA spreads were fixed in methanol/acetic acid (3:1). Prior to immunodetection, slides were treated with 2.5 M HCl for 1 h and 15 min. The slides were further incubated with rat anti-bromodeoxyuridine and mouse anti-bromodeoxyuridine for 1 h to detect CldU and IdU labeled tracts, respectively. Subsequently, slides were fixed in formalin solution for 10 min to increase staining intensity and further incubated with anti-rat IgG AlexaFluor 568 and anti-mouse IgG AlexaFluor 488 (Molecular Probes, 1:500) for 2 h. Slides were mounted with Fluoroshield (Sigma). Images were acquired with an AxioImager Z1 ApoTome microscope system (Carl Zeiss, Jena, DE) using a 63x (1.4 numerical aperture) oil lens, a AxioCam Mrm camera and the Axiovision 4.8.2 (Carl Zeiss) software. Images were analyzed using ImageJ (Schneider et al., 2012). In each independent experiment, at least 250 fibers were measured per condition. Replication track lengths were calculated using the conversion factor 1 μM = 2.59 kb (Jackson and Pombo, 1998).

GFP pulldowns and SILAC experiment

For SILAC GFP pulldowns, cells were grown for six cell divisions in DMEM containing L-arginine and L-lysine or L-arginine $^{13}C_6$ and L-lysine 4,4,5,5-D4 (Life Technologies). 24 h prior to harvesting, labeled cells were transiently transfected with EGFP alone or PNUTS EGFP. Nuclei were harvested, and GFP pulldowns performed as previously described with some modifications (Trinkle-Mulcahy et al., 2006). To increase efficiency of extraction of chromatin bound proteins, nuclei were resuspended in a high salt (500 mM NaCl) RIPA buffer for the sonication step and the resulting lysates diluted with NaCl-free RIPA buffer to a final concentration of 150 mM NaCl. Equal amounts of lysate (by total protein concentration) were mixed 1:1 and EGFP-tagged proteins isolated using

the GFP-Trap_A affinity matrix (Chromotek). Beads were washed and combined and proteins eluted for gel separation and trypsin digestion as previously described (Prévost et al., 2013). GFP pulldowns followed by western blotting were performed as the SILAC GFP pulldowns, but with the following modifications. Cells grown in regular medium were transiently transfected with EGFP PNUTS^{wt}, EGFP PNUTS^{RAXA}, EGFP TOX4, EGFP WDR82 or EGFP NIPP1 24 h prior to harvest. The cells were spun down and re-suspended directly in ice-cold high salt RIPA buffer (500 mM NaCl) and sonicated. The resulting lysates were diluted as above to 150 mM NaCl, and lysate volumes were adjusted to contain an equal amount of protein prior to isolation of EGFP-tagged proteins with GFP-Trap_Dynabeads (ChromoTek). The beads were washed five times in RIPA buffer (150 mM NaCl), diluted in 1x Lane Marker Reducing Sample Buffer (Pierce Biotechnologies) and were boiled (95°C, 5 min) prior to analysis by western blotting.

Mass spectrometry and data analysis

High-resolution mass spectrometric analysis was performed as described previously (Andersen et al., 2002) using a LTQ-FT-ICR mass spectrometer (Thermo Finnigan). Protein ratios were calculated for each arginine and lysine-containing peptide as the peak area of L-arginine $^{13}C_6$ and L-lysine 4,4,5,5-D4 divided by the peak area of L-arginine and L-lysine for each single scan mass spectrum. Peptide ratios for all arginine and lysine -containing peptides sequenced for each protein were averaged. The open source software MS-Quant was used to extract information from the Mascot HTML database search files (Matrix Science) and to evaluate the certainty in peptide identification and in peptide abundance ratio.

Phosphatase assay

Phosphatase assay was based on the method of Beullens et al. (Beullens et al., 1998) with modifications detailed below. RNAPII in isolated GFPpnuts complexes were used as substrate, and isolated as in the GFP pulldowns above with the following modifications. HeLa or HeLa GFPmpnuts were transfected with scr or siWDR82#3 and harvested after 72 h. Cells were resuspended in ice-cold TX-100 buffer (100 mM NaCl, 50 mM Tris pH 7.5, 2 mM $MgCl_2$, 0.5% TX-100) containing 100 U/ml Benzonase (Merck), Complete EDTA-free Protease Inhibitor Cocktail (Merck), PhosSTOP phosphatase inhibitors (Merck) and 50 μM MG132 (Sigma Aldrich). Lysates were precleared and GFPmpnuts complexes were isolated with GFP-Trap_Dynabeads (Chromotek). GFPmpnuts complexes were washed three times with TX-100 buffer containing 400 mM NaCl, and two times with PP1 buffer (20 mM Tris, 0.5 mM DTT, 1 mM MnCl2, 0.025% Tween-20, Complete EDTA-free Protease Inhibitor Cocktail and 50 μM MG132). Complexes were resuspended in PP1 buffer, aliquoted and placed at 30°C with gentle mixing (300 rpm) for the indicated times. Reactions were stopped by addition of PhosSTOP phosphatase inhibitors (Merck) and Lane Marker Reducing Sample Buffer (Pierce Biotechnologies), and samples were boiled prior to analysis by western blotting.

Live cell imaging

Live-cell imaging was performed on a Leica SP5 confocal laser scanning microscope with a HCX PL APO CS 63 ×, 1.40-NA oil-immersion lens. Images were recorded with a 488-nm Argon laser and a 500- to 600-nm bandpass filter. For FRAP, at pixel size 24.6 × 24.6 μM, a strip of 512 × 32 pixels spanning the nucleus was imaged every 400 ms with 400 Hz. Twenty-five frames were recorded before the bleach pulse. The average, background-corrected fluorescence intensity of frames 10–20 of these prebleach measurements were used to calculate the prebleach fluorescence intensity. GFP fluorescence in the strip was bleached for one frame with 100% laser power. The recovery of fluorescence was monitored for 4 min (600 frames) within and outside the strip, background-corrected, and normalized to pre-bleach fluorescence intensity.

Immunofluorescence

For detection of chromatin loaded RPA70 and γH2AX by immunofluorescence, HeLa cells were pre-extracted in detergent buffer (20 mM HEPES, pH 7.4; 50 mM NaCl; 1.5 mM MgCl2: 300 mM sucrose; 0.05% Triton X-100) for 5 min on ice prior to fixation with formalin solution (Sigma Aldrich). Coverslips were stained with anti-RPA70 and anti- γH2AX in PBS-AT (PBS with 0.5% Triton X-100 and 1% BSA), followed by anti-mouse Alexa Fluor 568 and anti-rabbit Alexa Fluor 488 (Thermo Fisher). Imaging and analysis was as previously described (Landsverk et al., 2019).

Clonogenic survival assay

For the clonogenic survival assay 200 HeLa cells were seeded in 6 cm culture dishes (BD Biosciences) with medium containing no drug or 50 μM or 100μM of hydroxyurea (Sigma Aldrich). On day 13 after seeding, 500 μL fresh medium was added to the dishes and the cells were cultured for an additional 6 days (19 days in total), fixed in 70% ethanol and stained with methylene blue. Colonies of 50 or more cells were counted as survivors. Survival fractions were calculated in each experiment as the average cloning efficiency (from 3 parallel dishes) after treatment with hydroxyurea, divided by the average cloning efficiency for non-treated cells.

Prognostic data

Prognostic data for PNUTS (PPP1R10) was found at the Human Protein Atlas available from http://www.proteinatlas.org

QUANTIFICATION AND STATISTICAL ANALYSIS

All experiments, except when otherwise stated, were performed three times or more. Error bars represent standard error of mean (SEM). P values were determined by the two-tailed student's two sample t test unless otherwise stated, and were determined using Microsoft Excel, except the Wilcoxon test, which was performed using Sigmaplot. *n* refers to number of independent experiments, except in Figure 4A, when it refers to number of cells analyzed. * < 0.05, ** < 0.01, *** < 0.001